

# Multi-site learning for ~~error-correction and~~ hydrological uncertainty prediction: the case of quantile random forests

Taha-Abderrahman El Ouahabi<sup>1</sup>, François Bourgin<sup>1</sup>, Charles Perrin<sup>1</sup>, and Vazken Andréassian<sup>1</sup>

<sup>1</sup>Université Paris-Saclay, INRAE, HYCAR, Antony, France

**Correspondence:** Taha-Abderrahman El Ouahabi (taha.elouahabi@gmail.com) and François Bourgin (francois.bourgin@inrae.com)

## Abstract.

To improve hydrological uncertainty estimation, recent studies have explored machine learning (ML)-based post-processing approaches that enable both enhanced predictive performance and hydrologically informed probabilistic streamflow predictions. Among these, random forests (RF) and their probabilistic extension, quantile random forests (QRF), are increasingly used for their balance between interpretability and performance. However, the application of QRF in regional post-processing settings remains unexplored. In this study, we develop a hydrologically informed QRF post-processor trained in a multi-site setting and compare its performance against a locally (at-site) trained QRF using probabilistic evaluation metrics. The QRF framework leverages simulations and state variables from the GR6J process-based hydrological model, along with readily available catchment descriptors, to predict daily streamflow uncertainty. Our results show that the regional QRF approach is beneficial for hydrological uncertainty estimation, particularly in catchments where local information is insufficient. The findings highlight that multi-site learning enables effective information transfer across hydrologically similar catchments and is especially advantageous for high-flow events. However, the selection of appropriate catchment descriptors is critical to achieving these benefits.

## 1 Introduction

### 1.1 On the need for quality uncertainty estimates

Providing quality uncertainty estimates for streamflow predictions is critically important, particularly in applications such as operational drought simulation, water resource management, and flood mitigation where significant stakes are involved (Hwang et al., 2019; White et al., 2017). Poorly quantified or overly confident predictions can lead to misinformed decisions, potentially resulting in economic losses, infrastructure damage, or even threats to public safety. To address this, various approaches have been proposed in the hydrological community for streamflow uncertainty quantification, including multi-model ensembles (Georgakakos et al., 2004; Troin et al., 2021), Bayesian inference (Kuczera and Parent, 1998; Bates and Campbell, 2001), and hydrological error modeling (Krzysztofowicz, 1999; Todini, 2008; Solomatine and Shrestha, 2009; Bennett et al., 2021), referred to as post-processing. Post-processing involves a process-based model followed by a statistical approach to correct er-

rors and quantify the associated uncertainties. With the post-processing procedure, uncertainties can be quantified by modeling  
25 the error patterns based on an archive of past data.

Hydrological post-processing techniques were adopted early through methods such as the hydrological uncertainty processor (HUP) (Krzysztofowicz, 1999) and model conditional processor (MCP) (Todini, 2008), but recent machine learning (ML)-  
based approaches have emerged as powerful tools for hydrological post-processing. Although less interpretable, ML-based  
approaches can potentially produce reliable and more informative uncertainty estimates (Papacharalampous and Langousis,  
30 2022; Tyralis and Papacharalampous, 2024). Methods such as quantile regression (QR) (Tyralis et al., 2019; Papacharalampous  
and Langousis, 2022), conformal prediction (Auer et al., 2024), and random forests (Zhang et al., 2023) have been used  
for streamflow post-processing with promising results. However, ML algorithms can produce different uncertainty estimates  
depending on how they are trained — particularly on which catchments are included in the training dataset. Since hydrological  
conditions vary significantly across catchments, the selection of catchments used for training can influence the uncertainty  
35 estimates of the ML model. In our study, we aim to explore whether including different catchments, referred to as regional or  
multi-site learning, may improve ML-based post-processing for error-correction and uncertainty prediction, and specifically  
for the quantile random forests (QRF) model. A QRF model for error-correction and uncertainty prediction trained in a regional  
setting can leverage information across several catchments. In contrast, local at-site approaches train models independently for  
each catchment and cannot benefit from error patterns shared in hydrologically similar catchments.

## 40 1.2 Machine learning-based post-processors

Random forest (RF) (Breiman, 2001) and its probabilistic variant, quantile random forest (QRF) (Meinshausen and Ridgeway,  
2006) are extensively used and are considered state-of-the-art in many hydrological applications. Recently, Zhang et al. (2023)  
compared the QRF model and the countable mixtures of asymmetric Laplacians long short-term memory (CMAL-LSTM)  
model to probabilistically post-process streamflow simulations across 522 catchments. The QRF and CMAL-LSTM models  
45 were comparable in terms of uncertainty estimates, but the CMAL-LSTM deep learning (DL) model performed better in catch-  
ments with large flow accumulation areas. QRF has also been applied in hydrologically informed post-processing approaches.  
Shen et al. (2022) use an RF framework and leverage internal state variables to correct ~~PCR-Global~~ PCR-GLOBWB (PCRas-  
ter Global Water Balance, a global hydrological model) simulations at three stations in the Rhine Basin. They found that the  
use of hydrological model states as input features of RFs provides additional information that may not be included in the  
50 model simulations. However, challenges remain, particularly in modeling errors during high streamflow periods. Magni et al.  
(2023) expand the same approach at a global scale, using ~~PCR-Global~~ PCR-GLOBWB model simulations and internal states,  
in conjunction with static catchment attributes, to train a single RF model on a global database of streamflow simulations and  
measurements. They found that improvements were independent of the availability of streamflow data, indicating the power of  
regional learning methods in poorly gauged and ungauged catchments.

55 Prediction in ungauged basins is not the only benefit of training a single ML model on data from multiple catchments.  
Kratzert et al. (2024) advocate the use of regional approaches to fit a deterministic Long Short-term Memory (LSTM) DL  
model for streamflow simulations. They found that larger LSTM models trained on all available basins outperform smaller

models trained on a limited set of catchments. This is because some ML approaches can properly use the additional information contained in larger training sets to perform better than models specialized for individual catchments (Montero-Manso and Hyndman, 2021). Furthermore, Johnson et al. (2023) found that hydrological model performance depends on catchment characteristics, indicating the presence of regional bias, where hydrological errors exhibit similar properties for neighbouring catchments. This can be harnessed to improve uncertainty estimation using a post-processing model with a regional parametrisation and trained on hydrological errors from multiple sites. We intend to consider these catchment characteristics as additional input features within the proposed post-processing model.

### 65 **1.3 Scope of this study**

This study addresses uncertainty estimation of process-based hydrological model simulations, with a focus on streamflow reconstruction and future projection scenarios. We investigate the added value of multi-site post-processing applied to a quantile random forests (QRF) model. The main contributions of this work are: (i) to understand the impact of including different catchments in the training process of QRF (multi-site) on the quality of its uncertainty estimates and (ii) to investigate the importance of catchment characteristics for these multi-site QRFs. Although multi-site approaches can benefit the modelling of ungauged catchments, our work specifically addresses improvements in uncertainty estimation for catchments with available streamflow measurements.

Accordingly, we use temporally varying information (predicted streamflows and model states) in addition to catchment dependent characteristics to estimate uncertainties in hydrological model predictions. We chose to focus on QRF due to its balance of performance, interpretability, and popularity in the hydrological community. To the best of our knowledge, no prior study has explored the impact of multi-site learning with the QRF algorithm for uncertainty estimation, particularly when post-processing a hydrological model calibrated separately for each catchment. To that end, we fit different QRF variants on the internal states of a hydrological model, on meteorological variables, and on readily available catchment characteristics. The proposed regional QRF variants are evaluated across a large sample of 564 French catchments to identify when multi-site learning may be beneficial and to offer practical considerations for multi-site QRF applications.

The paper is organized as follows: We first introduce the dataset and describe the QRF algorithm, its variants, and the probabilistic evaluation framework. Then, we present and discuss the results before summarizing the key findings along with implications for future work.

## **2 Dataset**

### 85 **2.1 A dataset of 564 French catchments**

We used a set of 564 catchments distributed throughout France (Fig. 1). These catchments represent a wide range of hydrological regimes and simulation contexts. We selected these catchments from the CAMELS-FR hydroclimatic dataset (Delaigue et al., 2024). The criteria for selecting these catchments were as follows: (i) low anthropogenic influence, (ii) good data quality

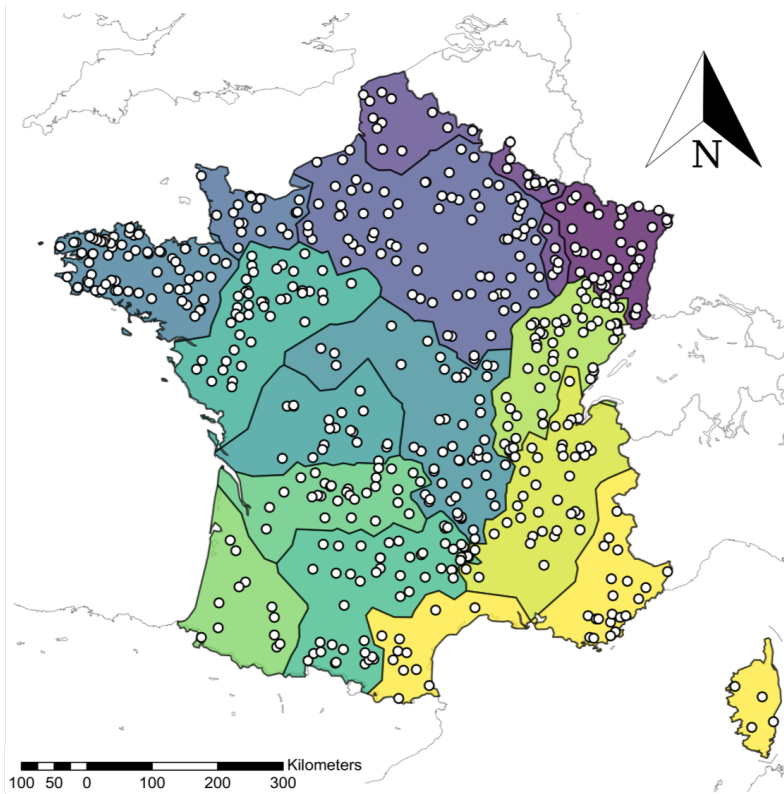


**Figure 1.** Location of the 564 catchment outlets. Plotted regions represent the hydroclimatological catchment groups used in the study.

for all flow regimes, and (iii) an available time series longer than 21 years. Streamflow data were obtained from the national  
 90 HydroPortail archive (Leleu et al., 2014; Dufeu et al., 2022) at a daily time step for the period 1977–2021. Meteorological  
 forcings (precipitation and temperature) were provided by Météo-France’s daily SAFRAN grid reanalysis (Vidal et al., 2010).  
 Potential evaporation (PET) is calculated using the formula proposed by Oudin et al. (2005) and requires two inputs: extrater-  
 restrial radiation ( $MJ/m^2/day$ ) and mean daily air temperature ( $^{\circ}C$ ). Extraterrestrial radiation is computed as a function of  
 the localization of the basin and Julian day values and the temperature is the only dynamical meteorological input used to esti-  
 95 mate PET. Since our interest is in developing a multi-site QRF post-processor, we used several static basin-averaged attributes  
 describing climate, topography, and geology. All of these attributes are included in the CAMELS-FR dataset and are listed in  
 Table 1.

Hydrological calibration was performed independently for each catchment over the 1977–2021 period. Subsequently, the  
 QRF variants were implemented using a standard train–validation–test split over the 1990–2021 period:

- 100 – **P1:** training period from 1990 to 2004, used to train the QRF post-processor.
- **P2:** validation period from 2005 to 2009, used to select the hyperparameters of the QRF post-processor.

– **P3**: testing period from 2010 to 2021, used to test the performance of the QRF variants on new data.

## 2.2 Methods

### 2.3 Hydrological model

105 We used discharge simulations obtained with the GR6J rainfall–runoff model (Pushpalatha et al., 2011), a daily 6-parameter conceptual lumped model. GR6J has been applied in several studies across a large number of catchments and hydroclimatic contexts (e.g. Poncelet et al., 2017; Golian et al., 2021; Tanguy et al., 2023). The GR6J model is based on several state variables that control its simulations, in particular, the production and routing store levels, as well as intercatchment exchange fluxes. We intend to use these state variables as predictors in the QRF algorithm. Shen et al. (2022) successfully used internal state variables as predictors in an RF framework to correct hydrological model errors. They found that internal state variables provided valuable information for the RF, enabling it to detect and correct for systematic hydrological model errors. To account for the influence of snow in some catchments, we incorporated Cemaneige (Valéry et al., 2014), a snow accumulation and melt model, with constant parameters for all catchments.

115 The Cemaneige-GR6J model was calibrated using the airGR R package (Coron et al., 2017, 2023) using the built-in calibration algorithm. To ensure good performance across a wide range of streamflow conditions, the target optimization criterion was a combination of KGE based criteria (Gupta et al., 2009; Kling et al., 2012): an equal weighting of KGE criteria with power transformations of 0.5 and -0.5 applied to streamflow, as detailed in Appendix C. This calibration approach was implemented to obtain the six parameters of GR6J: production store capacity (*mm*), groundwater exchange coefficient (*mm/day*), routing store capacity (*mm*), time constant of unit hydrograph (*days*), groundwater exchange threshold (–), and exponential store coefficient (*mm*).

### 2.4 Feature selection and data transformations

#### 2.4.1 Target variable

For this study, we model the probabilistic distribution of hydrological model errors. Since these errors are skewed and non-Gaussian (e.g. Evin et al., 2014), we applied a logarithmic transformation to improve the training process:

$$125 \quad \epsilon_t = \log\left(\frac{Q_t^{obs} + \delta}{Q_t^{sim} + \delta}\right) \quad (1)$$

where  $\epsilon_t$  is the target variable of our study and represents the prediction error,  $Q_t^{obs}$  and  $Q_t^{sim}$  indicate observed and simulated streamflows, respectively (mm/day), and  $t$  represents the time index with a temporal step of 1 day.  $\delta$  is an offset parameter to avoid zero streamflow values and is unique for each catchment. It was calculated following the recommendation in Pushpalatha et al. (2012). The use of  $\delta$  is especially relevant in this study due to the application of the logarithmic transformation.

130 The input predictors (or features) in the QRF models are listed in Table 1. These features can be broadly categorized into two groups of approximately equal size: (i) time series data (dynamic features) that capture temporal variability, and (ii) catchment descriptors (static features) that enable spatial identification of catchments.

### 2.4.2 Dynamic features

The proposed QRF framework post-processes GR6J simulations and uses hydrological model outputs and state variables along with meteorological inputs (precipitation and temperature). Streamflow uncertainties are known to be autocorrelated (Evin et al., 2014), with strong autoregressive (AR) and memory effects. Consequently, lagged observed streamflow (Zhang et al., 2023; Pham et al., 2020) is a popular input feature for RF-based post-processing. In the simulation context of this study, streamflow observations are not available for streamflow reconstruction and projection scenarios, and we use state features from the GR6J model to provide additional information to QRF. Although some of the features in Table 1, such as simulated flows and production store, are strongly autocorrelated, we assume that the additional information still leads to improved uncertainty estimates compared to using model simulations alone. Similarly to (Shen et al., 2022), we include other temporal information in QRF through transformed features: (i) increment features of hydrological model simulated streamflow and states to help capture the dynamics of the hydrograph (rising and falling limbs etc.) and (ii) moving averages of meteorological features to highlight general trends. This feature engineering step can be relevant for RF-based algorithms in a time series context, because QRF does not create temporal memory or embeddings as is the case for AR models and LSTM neural networks (Evin et al., 2014; Li et al., 2016; Kratzert et al., 2018). In this context, the selected moving average filter size is equal to the catchment response time, which was obtained from the time constant of the unit hydrograph parameter of the GR6J model.

### 2.4.3 Static features

To take into account spatial heterogeneity, catchment descriptors are used for the multi-site QRF variants. The static features include (i) average catchment attributes such as catchment area and aridity index. We chose to keep thirteen relevant catchment attributes following the recommendations of Jehn et al. (2020); (ii) scale features of errors, simulated flows, and observed streamflows. These scale features provide additional unique indicators of catchment characteristics. Montero-Manso and Hyn-dman (2021) found that combining individual time series features such as catchment attributes with scale features can improve the performance of ML models in a deterministic setting. Similar improvements are expected for QRF in the setting of hydro-logical uncertainty estimation. It is important to note that these scale features are not available for prediction in the context of ungauged catchments, as they are calculated based on observed streamflows.

## 2.5 QRF: how to fit the algorithm?

Random forest Breiman (2001) is a non-parametric ensemble tree-based model that offers good performance and provides certain interpretability through its feature importance estimates (Breiman, 2001; Breiman et al., 2017). RF and its probabilistic version QRF are used extensively in the hydrometeorological domain. An important advantage of QRF is that it provides full

**Table 1.** Features used in the study

Features	Unit	Description	Type
PotEvap	mm/day	potential evapotranspiration	
Precip	mm/day	precipitation	
AE	mm/day	actual evapotranspiration	
Prod	mm	production store	
Rout	mm	routing store	
AExch	mm/day	intercatchment exchange	
Qsim	mm/day	simulated flows	
Delta_sim7	mm/day	7-day difference in simulated flows	
Delta_sim1	mm/day	1-day difference in simulated flows	
Delta_rout7	mm	7-day difference in routing store	<b>Dynamic features</b>
Delta_rout1	mm	1-day difference in routing store	
Delta_prod1	mm	1-day difference in production store	
Prec_sold_frac	-	fraction of solid precipitation	
Temp	°C	temperature	
SWI_ISBA	-	soil wetness index	
Rolling_temp	°C	moving average of temperature	
Rolling_precip	mm/day	moving average of precipitation	
Rolling_sold_frac	mm/day	moving average of solid precipitation	
Month_of_year	-	annual cycle (cosine term)	
top_drainage_density	-	drainage density	
sit_area_topo	km <sup>2</sup>	topographic catchment area	
hyd_bfi_pelletier_pet_ou	-	baseflow index	
cli_prec_mean	mm/day	mean daily precipitation	
cli_pet_ou_mean	mm/day	mean daily potential evapotranspiration	
cli_temp_mean	°C	mean daily temperature	
cli_aridity_ou	-	aridity index	
cli_psol_frac_safran	-	mean fraction of solid precipitation	
cli_prec_freq_high	-	frequency of high-precipitation days	
cli_prec_freq_low	-	frequency of dry days	
top_altitude_mean	m	mean catchment elevation	<b>Static features</b>
cli_prec_season_pet_ou	-	seasonality index	
Response_Time	days	Response time based on the X4 parameter from GR6J	
mean_Qsim	mm/day	mean Qsim	
std_Qsim	mm/day	standard deviation of Qsim	
mean_Qobs	mm/day	mean Qobs	
std_Qobs	mm/day	standard deviation Qobs	
mean_Error_log	-	mean error log	
std_Error_log	-	standard deviation error log	
Region indicator	-	Hydroclimatological region of the catchment	

distributional estimates without the need to estimate each quantile separately, as is required in quantile regression (Tyrallis et al., 2019; Papacharalampous and Langousis, 2022). QRF has been applied to complex and heteroscedastic cases, including hydrometeorological ensemble forecasts (Taillardat et al., 2016; Tiberi-Wadier et al., 2021; Teja et al., 2023), post-processing of streamflow simulation (Zhang et al., 2023), and estimation of the limits of acceptability for hydrological models (Gupta et al., 2024). Further details on the construction of RF and QRF can be found in (Louppe, 2014; Meinshausen and Ridgeway, 2006), but, QRF can be viewed as an analog method (Delle Monache et al., 2013; Hu et al., 2023) that performs a weighted nearest-neighbor search for analogous events. Similarly to a classic RF, QRF grows a number of trees  $n$ , with each tree trained on a bootstrapped subsample of the original training data.

Individual trees are trained according to the Breiman et al. (2017) algorithm by minimizing a loss function and making successive splits with a predefined number of features  $p$ . This tree-building process enables QRF to account for strongly correlated features, which is important given the strong correlation of some of the features used. For the purpose of this study, we use mean squared error (MSE) as a loss function to calculate the homogeneity of each group. The procedure continues recursively, with each resulting group split further until a minimum number of data points  $m$  in child splits is reached.

In the classic Random Forest (RF) algorithm, predictions from individual trees are averaged to produce a single deterministic output. In contrast, Quantile Regression Forest (QRF) leverages the leaf nodes of trees to compute proximity measures between a test input and training instances. For a prediction at time  $t$  and given input  $x_t$ , each QRF tree is traversed using binary splits to reach a corresponding leaf node. A proximity weight  $\omega_i(x_t)$  is then defined for each training instance  $i$  (Meinshausen and Ridgeway, 2006), which is then used to estimate the cumulative distribution function (CDF) of the prediction uncertainty:

$$\hat{F}(\epsilon|x_t) = \sum_{i=1}^n \omega_i(x_t) \mathbb{1}_{\{\epsilon_i \leq \epsilon\}} \quad (2)$$

where  $\omega_i(x_t) > 0$  and  $\sum_{i=1}^n \omega_i(x_t) = 1$ ,  $\epsilon_i$  denotes the hydrological error of training instance  $i$ , and  $\hat{F}$  is the estimated CDF of uncertainty for  $x_t$ .

To provide reliable and sharp uncertainty estimates, we considered three hyperparameters for optimization: (i) The minimum number of samples at child nodes  $m$ , which affects tree depth and strongly impacts reliability and sharpness. Setting high values for the minimum samples per leaf might yield high reliability, but can lead to poor performance, as the trees are too general and information is lost. Low values result in overfitting and unreliable uncertainty estimates. (ii) The number of features per split,  $p$ , which also shapes the QRF uncertainty estimates. Higher values can lead to under-dispersed uncertainties, while lower values may reduce sharpness. (iii) The number of trees  $n$ , which controls precision and stability. A larger number of trees improves the quality of uncertainty estimates, but improvements diminish as computational cost increases, especially in larger models. Further details on hyperparameter values and selection are provided in Section 2.7. Additionally, we also use a K-nearest neighbor (K-NN) (Wani et al., 2017) approach as a benchmark for the QRF methods used in the study. Like QRF, K-NN aims to find analogous events but based on the Euclidean distance between features. Here, K-NN is fitted locally on the same variables as for QRF. Further details on the fitting process and the hyperparameters used are provided in Appendix B.

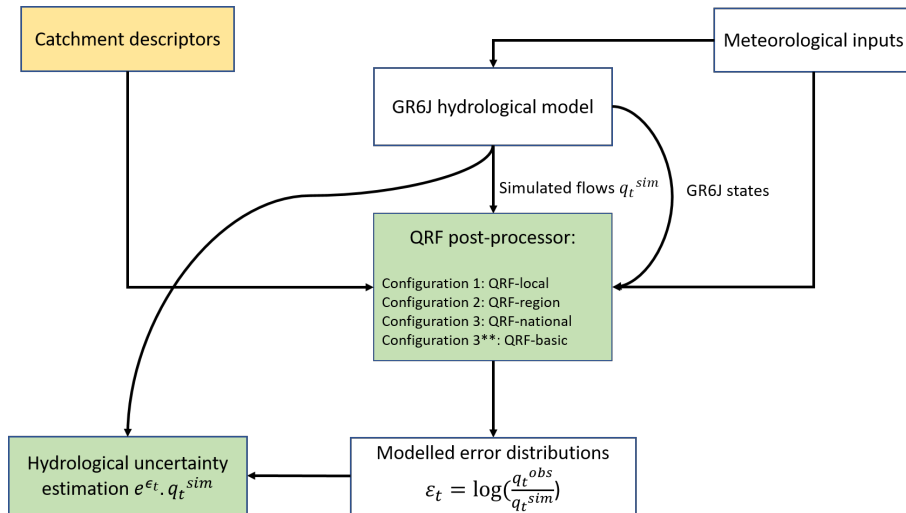


**Figure 2.** Schematic overview of implementing QRF based post-processors. Configurations 1, 2, and 3 represent the regional information used in QRF post-processing. A description of the features used is provided in Table 2.

Given equation (2), the estimated CDF is bounded by the training sample. QRF is unable to predict a quantile higher than the maximum observed in the training sample, which implies that QRF trained on a single basin is constrained by the range of errors in its training data. A more hydrologically diverse training dataset would alleviate this problem and enable QRF to adapt to more extreme events, provided that QRF is able to use the additional information properly.

## 2.6 QRF variants

Figure 2 presents the framework employed for the QRF configurations analyzed in this study. The local approach (QRF-local) refers to training the QRF algorithm on data from a single basin. Given their construction, spatial features are constant for each individual catchment and only time-series features can be fed to QRF in the local setup. QRF-local yields 564 independently trained QRF models, each specific to its respective catchment. Next, spatial variability is added as we extend QRF to a multi-site setting. The objective here is twofold: (i) to examine whether spatial diversity can improve the uncertainty estimates of QRF. This can be challenging, particularly since the used GR6J hydrological model is calibrated on an on-site basis; and (ii) to determine the optimal number of catchments to include in the training set for effectively capturing hydrological diversity and improving QRF predictions. We test QRF with two spatial settings: (i) a regional approach (QRF-region), where QRF is trained on data from catchments that are geographically close and thus potentially have similar error dynamics. In total, 15 regional QRF models are developed for the hydrological regions of the study (see Figure 1), based on hydroclimatological groupings of French catchments; (ii) a global approach (QRF-national), in which a QRF is trained on data from all catchments in the dataset. Both static and dynamic descriptors are used in the training process of QRF-region and QRF-national. However, QRF-national uses the catchment's hydrological region as an additional input feature, which cannot be used for QRF-region.

Intuitively, in cases where QRF is unable to transfer information from different basins or when there are no useful analogs in similar catchments, QRF-local would yield better performance, as no information from other catchments is used to build the model. To assess the usefulness of static features for the multi-site QRF setup, we included QRF-basic, a global QRF approach fitted on all catchments of the study, but only with dynamic features. This experiment is expected to highlight whether dynamic time series features are sufficient to improve multi-site QRF predictions or that static features are essential for multi-site post-processing. Table 2 presents the features used in the three configurations. The QRF models used in this study was fitted using the quantile-forest Python library (Johnson, 2024).

It is worth mentioning that in multi-site setups, the standardization procedure is an essential step that enables QRF to determine analogs across a set of diversified catchments, as the scales of streamflows and dynamic features (GR6J states and transformed variables) vary significantly. Standardization is important for a meaningful training process and for the identification of adequate analogous events. Initially, we standardized input data via the popular standard scaling method (Hastie et al., 2001), which transforms dynamic features – for each catchment – so that the average and standard deviation are set to 0 and 1, respectively. However, the method resulted in inconsistencies for catchments with outliers, as the standard deviation is sensitive to extreme values. To solve this issue, we opted for robust standardization (Hastie et al., 2001), which removes median values of dynamic features and the target errors  $\epsilon_t$  defined in Section 2.3.

**Table 2.** QRF variants of the study

Configurations	Dynamic features	Static features	Hydroclimatological group	Number of models
QRF-local	✓			564
QRF-regional	✓	✓		15
QRF-national	✓	✓	✓	1
QRF-basic	✓			1

## 2.7 QRF hyperparameters

Since we use QRF for probabilistic predictions, hyperparameter selection was based on the mean of the alpha score and CRPSS values. This would enable a selection based on the quality of overall uncertainty estimates with an emphasis on reliability. For QRF-local, hyperparameters were tuned independently for each catchment and the set maximizing the aforementioned criteria during the validation period was selected. QRF-region and QRF-national hyperparameters were selected based on median criteria among the regions' catchments. The selection criteria for QRF-local are specific to each catchment, which is expected to enhance the results of the local model compared to approaches that use fixed hyperparameters across multiple catchments. Table 3 presents the hyperparameters selected for optimization.

**Table 3.** Hyperparameters set optimized for QRF

Hyperparameter	Values
Min samples leaf	5, 10, 25, 50, 75, 100, 150, 200, 400, 600
Number of estimators	200, 400, 600
Max features	sqrt, 8, 16
Seeds	0, 1, 2

### 3 Assessment criteria

235 In this section, we present the probabilistic metrics used to evaluate the three variants of QRF. The criterion followed for proba-  
 bilistic predictions conforms to Gneiting et al. (2007)’s objective of maximizing reliability subject to sharpness. In this context,  
 reliability refers to the statistical consistency between the predicted uncertainty distributions and the observed streamflow val-  
 ues, while sharpness is a property of predictions exclusively and refers to the magnitude of the uncertainty distributions. In  
 practice, uncertainty estimates that closely align with observed streamflows are more accurate and reliable, while predictions  
 240 with smaller magnitudes are considered sharper. To assess these properties, we used two types of metrics. Distributional met-  
 rics evaluate the full predictive distribution, while interval metrics focus on a pre-specified predictive interval. As presented  
 below, reliability is measured by the alpha score and the coverage ratio. For assessing sharpness, we used the dispersion score  
 and average width interval. Additionally, deterministic evaluation criteria were also used to provide a more holistic assessment  
 of the proposed QRF variants. Each variant predicts 200 quantile members at each time step 200 quantile members equally  
 245 spaced between 0.005 and 0.995. The scores are calculated using the EvalHyd (Hallouin et al., 2023) Python library.

#### 3.1 Distributional metrics: alpha score, dispersion score, and CRPSS

The alpha score (Renard et al., 2010) targets reliability. It calculates the closeness of predicted uncertainty distributions to  
 the statistical distribution of observed streamflows. If the uncertainty distributions of streamflows are reliably quantified, the  
 observations correspond to realisations from the uncertainty distributions of streamflows. In practice, the alpha score compares  
 250 the empirical distribution of the probability integral transform (PIT) values to the uniform distribution on  $[0,1]$ . A perfect alpha  
 score corresponds to uniform PIT distributions while deviations of PIT values from the uniform distribution indicate lower  
 reliability. The values of the metric range from 0 (worst reliability) to 1 (perfect reliability).

For sharpness, we used the dispersion score calculated as a skill score following Bontron (2004). The method consists in  
 computing the continuous ranked probability score (CRPS; Gneiting et al., 2005) by comparing uncertainty distributions with  
 255 their medians, as detailed in Appendix E. This formulation targets the magnitude of the distributions instead of the agreement  
 with the observations. To obtain a positively oriented score, the dispersion score is expressed as a skill score by dividing by the  
 same quantity computed for the climatological distribution. The resulting metric scores 1 for a perfect point prediction; positive  
 values indicate better sharpness compared to the climatological distribution, while negative values indicate worse performance.

We also compute CRPS by comparing uncertainty distributions to observed streamflow values, which allows to assess both reliability and sharpness. We express CRPS as a skill score (CRPSS) relative to the climatological distribution, and similarly to the dispersion score, CRPSS equals 1 for perfect point prediction; positive values indicate better performance than the climatological distribution, while negative values indicate worse performance. Throughout the study, the empirical distribution of observed streamflows is defined over the training period, as detailed in Appendix E.

### 3.2 Coverage ratio, average interval width, and Winkler score

To provide a more comprehensive assessment of predictive uncertainty, evaluation metrics were calculated for prediction intervals at the 90% and 95% confidence levels. The coverage ratio (CR) is a measure of reliability that counts the proportion of observations that lie within the prediction intervals. Values closest to the desired coverage level (i.e., 90% or 95%) are best. Scoring lower values diminishes the utility of the model (under-coverage), while scoring higher values than the desired coverage is less problematic, but indicates that the model can provide sharper intervals (over-coverage). Moreover, it is worth highlighting that the two metrics used to assess reliability are closely related: the coverage ratio reflects reliability at a specific confidence level, while the alpha score aggregates coverage across all confidence levels. To assess the sharpness, we employ the average width metric (AW), which corresponds to the average width of the prediction interval during the evaluation period. We also evaluate the Winkler score (WS), which simultaneously includes both criteria, and enables an easy comparison between the variants of the study. Both AW and WS are presented as skill scores - AW skill score (AWSS) and Winkler skill score (WSS) - relative to the climatological distribution.

### 3.3 Deterministic metrics

Although the main focus of this study is probabilistic post-processing, some decision-makers may require deterministic predictions. Therefore, we also evaluate mean predictions to compare the different post-processing variants of the study. We use the popular Nash–Sutcliffe efficiency (NSE) (Nash and Sutcliffe, 1970) and Kling–Gupta efficiency (KGE) (Gupta et al., 2009) metrics to gauge the quality of deterministic predictions in multi-site learning setups.

## 4 Results

In this section, we compare each QRF variant according to its performance during the testing period. We investigate flow ranges in which multi-site learning is preferable, and we explore the importance of including catchment descriptors for regional QRFs. The results for the K-NN approach can be found in Appendix B. Figure. 3 illustrates the uncertainty estimates of QRF-local for a randomly selected catchment.

### 4.1 Hyperparameter tuning

We conducted a hyperparameter grid search for each QRF variant ~~and used the aforementioned selection criterion combining the using an equal contribution of the~~ alpha score and CRPSS ( $\frac{\alpha + CRPSS}{2}$ ) ~~as mentioned in section 2.7~~. Figure. 4 shows the

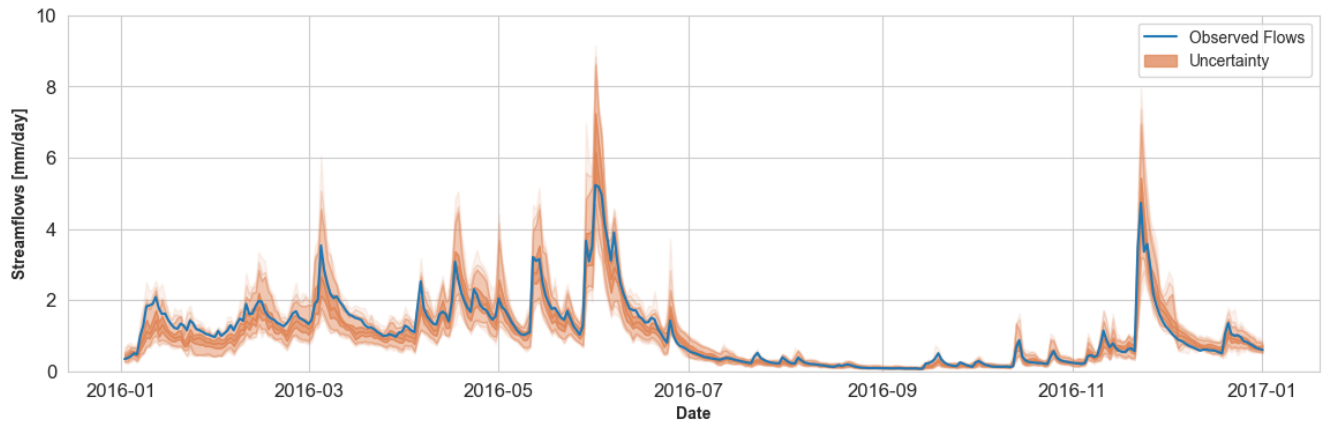


**Figure 3.** Example randomly selected for (station code K287191001 at Giroux with 756 km<sup>2</sup>) a catchment between 1<sup>st</sup> January 2016 and 1<sup>st</sup> January 2017 comprising both high- and low-flow events. Uncertainty estimates from QRF-local (orange) are plotted with the observed flows (blue). ~~Darker~~ The orange line represents the median of uncertainty estimates, while darker orange shades indicate regions of higher probability (25% and 75% quantiles). Lighter regions indicate low probability quantiles (5% and 95% in addition to 2.5% and 97.5% quantiles).

hyperparameter tuning procedure for QRF-national's three hyperparameters: the minimum number of samples at child nodes, the maximum number of candidate variables to use for splitting at each tree node, and the size of the forest (number of trees). We aim to obtain a single set of hyperparameters, and the selection criterion is based on the median of the alpha score and CRPSS across all catchments of the study. Each subplot illustrates how the selection criterion varies with the hyperparameter under consideration, while the variability reflects the influence of the remaining hyperparameters. This allows to assess the sensitivity of the QRF-national to each hyperparameter during the optimisation process. Overall, the performance of QRF was most sensitive to the minimum number of samples at child nodes. QRF was trained with minimum number of samples at child nodes ranging from 5 to 600 data points.

It is notable that best results were recorded for lower values of the minimum samples at leaf nodes. The improvement slows for values lower than 25. As such, a minimum samples at leaf nodes of 10 is selected. Overall, QRF was found to be fairly insensitive to the number of candidate predictors used for splitting at each node. By default, the quantile-forest library uses the integer value of the square root (sqrt) of the total number of predictors for this parameter. With 31 total predictors for QRF-national, 6 would be the default. Figure 4 shows that using the default value of the square root was slightly better. For the number of trees parameter, a forest with more trees will generally be more skillful than one with fewer trees, as it can fit on the nuances of the training set, and there is a point when the rate of improvement with more trees is negligible, as noted in Oshiro et al. (2012); Breiman (2001). Most of the boxplot ranges overlap, and the results appear to be relatively insensitive to this QRF parameter over the range considered.. For the experimented values, Figure 4 shows that a number of 400 trees allows for slightly better performances. We selected hyperparameters for the other QRF variants using a more specific basis: per

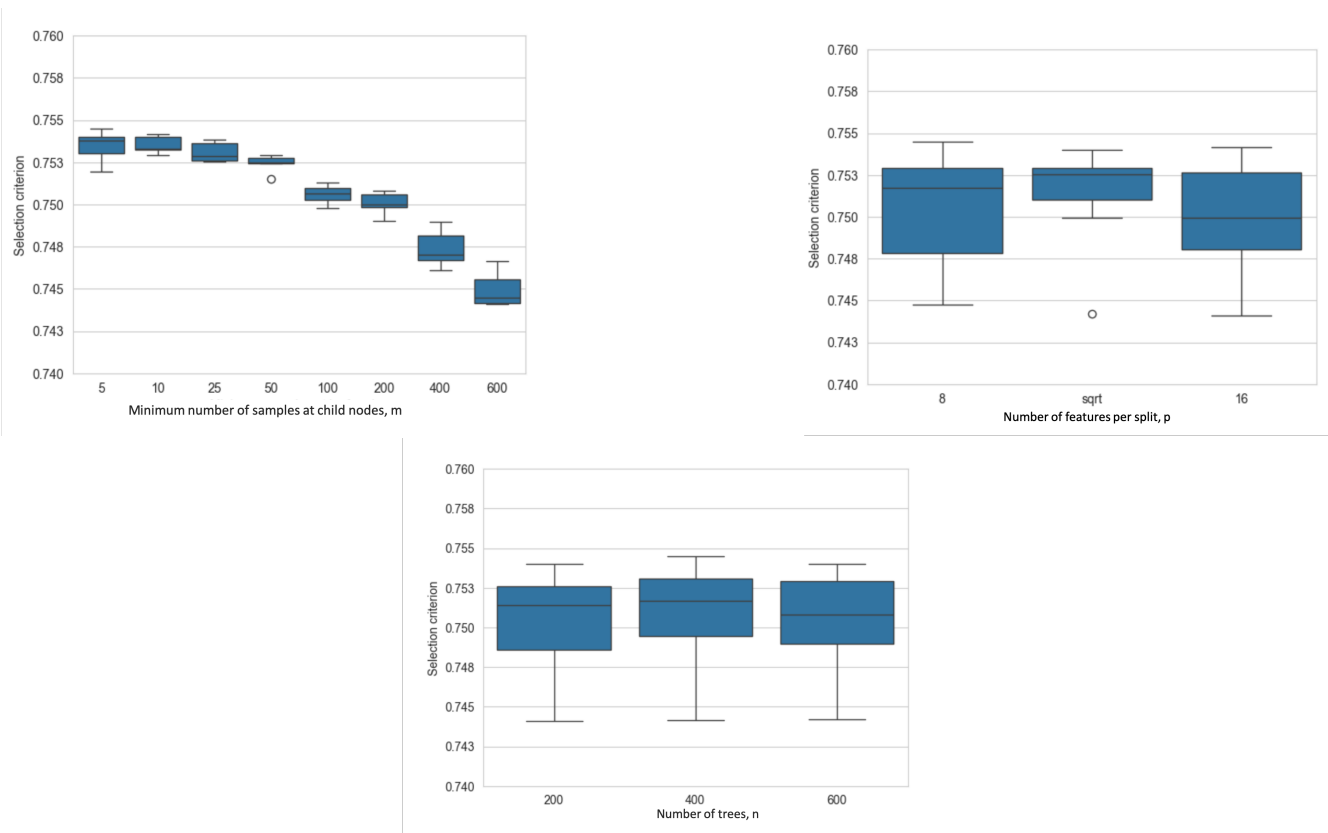


**Figure 4.** Hyperparameters optimization results for QRF-national. The selection criterion is the median hyperparameter criterion [with equal contribution of the alpha score and CRPSS](#) across the catchments of the study.

catchment for QRF-local and per region for QRF-region. One can expect that catchment specific hyperparameter tuning might help model performance. The distribution of the selected hyperparameters for QRF-local and-region is provided in [Appendix D, as mentioned in Sec. 2.7.](#)

#### 310 4.2 Alpha score, Dispersion score, and CRPSS

We first present our results with distributional metrics in Figure 5, which shows the cumulative distribution of reliability, sharpness, and CRPSS for the 564 catchments of the study. QRF-region and QRF-national slightly improve reliability compared to QRF-local. However, multi-site learning does not yield better alpha scores for well-calibrated stations with QRF-local. Figure 6 shows a direct comparison of the proposed variants and indicates that improvements were most noticeable for catchments where QRF-local provided low reliability, i.e., 25% of the basins with the lowest alpha scores (the 25% quantiles of the alpha score were 0.742 for QRF-local and 0.76 and 0.76 for QRF-region and QRF-national, respectively). In terms of sharpness, the different QRF variants performed similarly, while multi-site setups significantly improve CRPSS values. Among the QRF

variants, QRF-national generally outperformed QRF-local, improving CRPSS by approximately 2%, except in the case of four catchments, where QRF-local performed significantly better. Additionally, QRF-region improved CRPSS for 69% of the catchments compared to QRF-local, while QRF-national showed improvements in 88% of the catchments. Overall, the improvements are less apparent for reliability, but multi-site QRFs seem to improve performance for catchments with initially limited reliability in the local setup. As highlighted in Section. 3 CRPSS improvements combines both reliability or sharpness. Given that the sharpness metric was nearly identical across the QRF variants in the study, we suspect that the CRPSS improvements are mainly due to improvements in reliability. This is noteworthy, as the objective of probabilistic predictions is to improve reliability prior to enhancing sharpness (Gneiting et al., 2007).

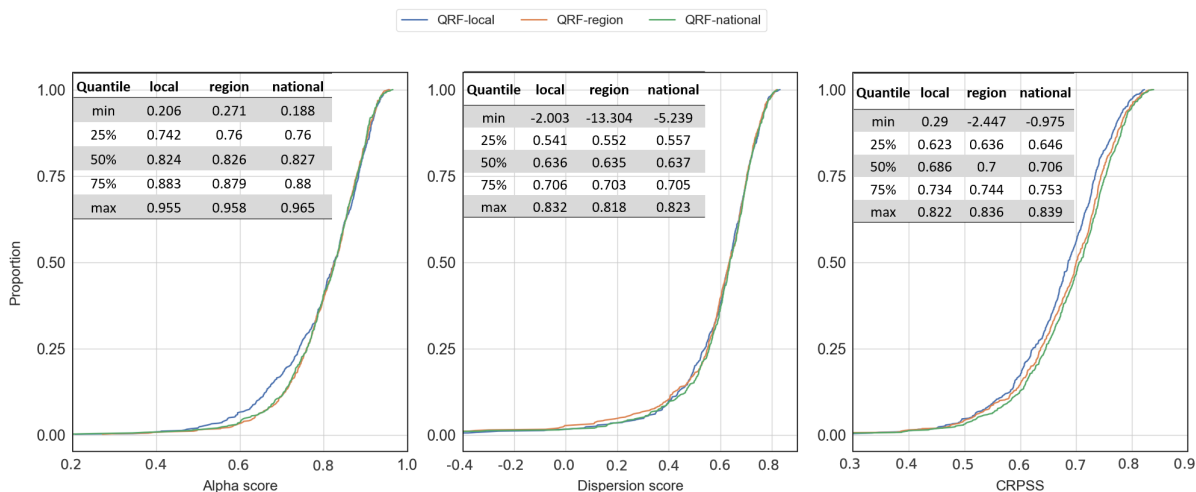


**Figure 5.** CDF of distributional metrics across the 564 catchments for the QRF variants in the study. Curves that are closer to the right of the plots indicate better performance. The blue line represents the performance of QRF-local, orange represents QRF-region, and green represents QRF-national.

### 4.3 Interval metrics

We now consider the 90% interval metrics. Figure 7 represents the box plots across the 564 catchments of the study for coverage ratio, average interval width, and Winkler skill scores. The multi-site learning setup was beneficial for QRF and improved the reliability of the predictive intervals. For instance, the median coverage ratios were set at 0.87, 0.89, and 0.89 for QRF-local, QRF-region, and QRF-national, respectively. Similar to the alpha score, the improvements in the multi-site QRF variants are most noticeable for stations with low reliability in the local approach. As shown in Figure 7, prediction intervals from multi-site QRFs over-cover observed streamflows (coverage ratio greater than 0.9) for certain catchments. While not optimal, this is a preferable outcome compared to the local approach, where uncertainty intervals more frequently miss the observed streamflows and tends to underestimate uncertainty in some catchments. The improvements are also observed for Winkler skill score, where QRF-national provided the best results. The average interval width was similar for all the variants

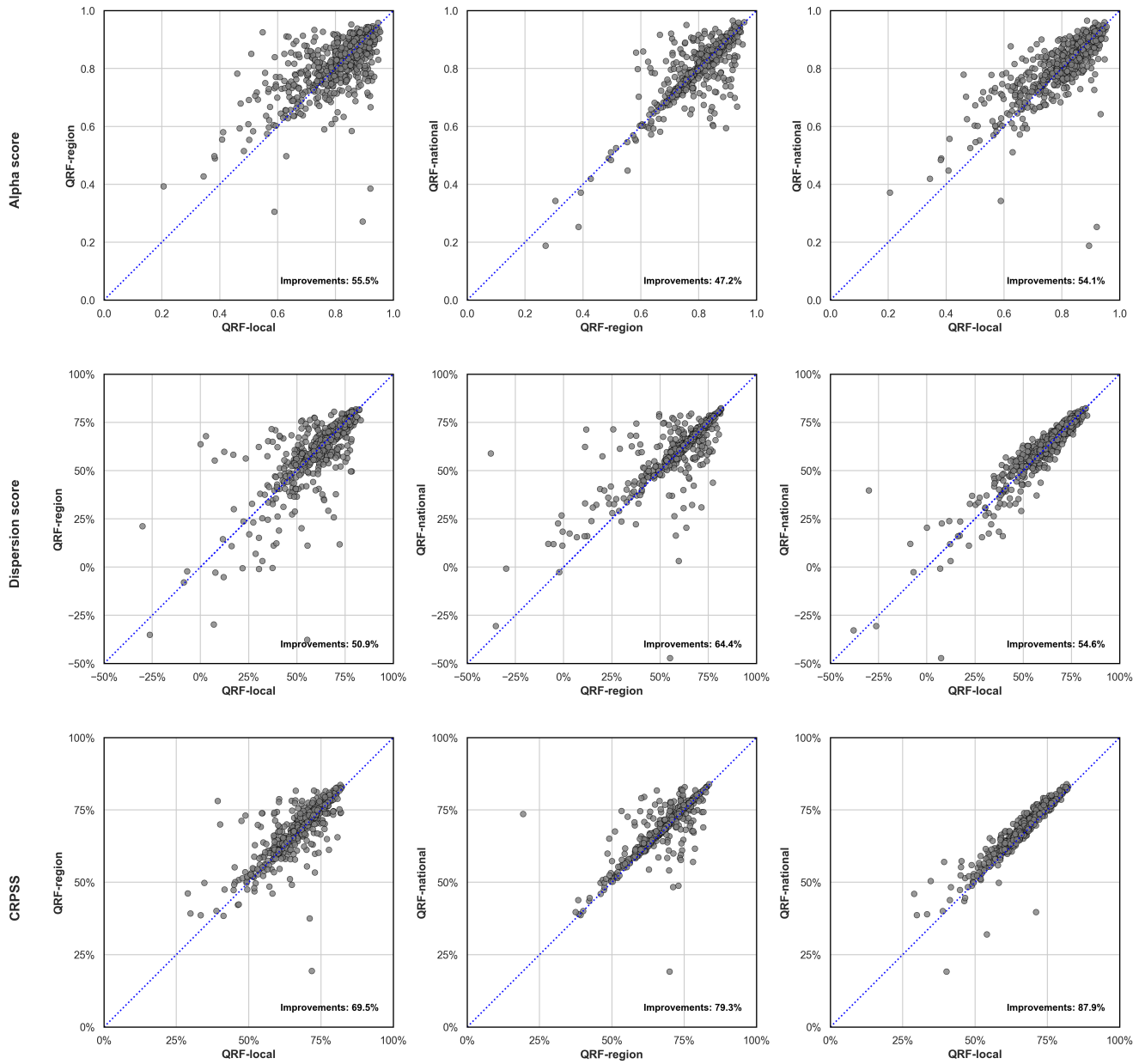


**Figure 6.** Comparative plots between QRF variants in the study during the testing period. The first row shows the alpha score, the second row shows dispersion, and the third row shows CRPSS. The first column compares metric values for QRF-local vs. QRF-region, the second column for QRF-national vs. QRF-region, and the third column for QRF-national vs. QRF-region

in the study, further indicating that improvements in multi-site learning in the case of QRF mainly relate to reliability. For the

sake of completeness, we include interval metrics for the 95% predictive uncertainty interval in Appendix F, as the conclusions remain the same.

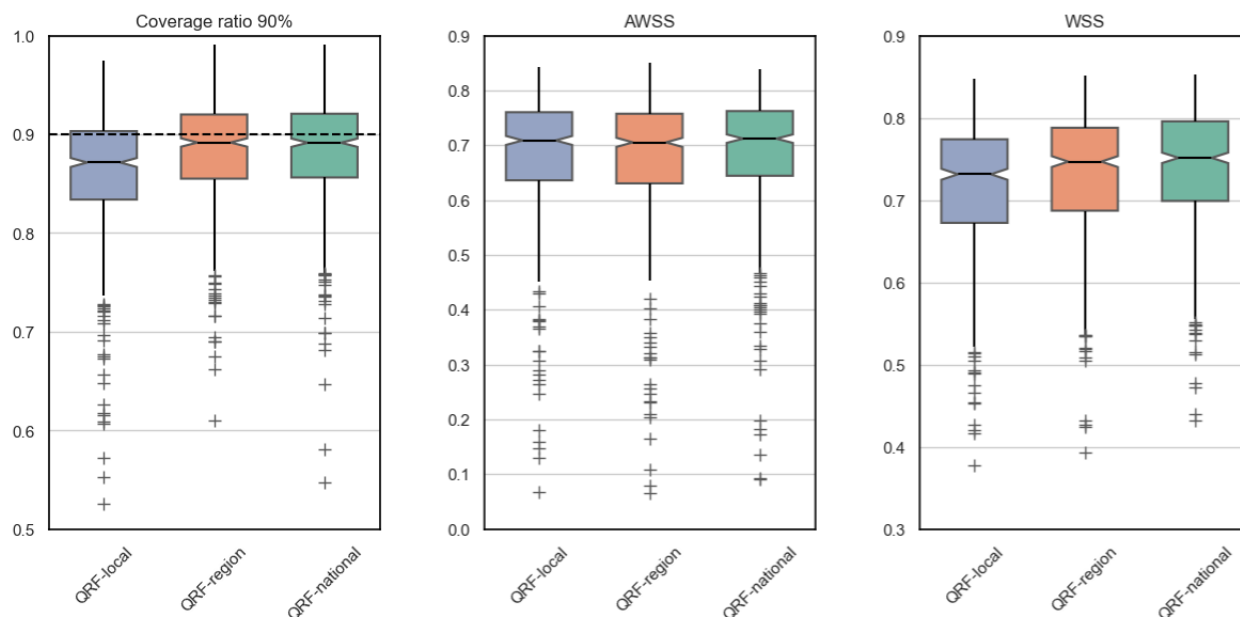


**Figure 7.** Box plots of 90% interval-based metrics across the 564 catchments of the study. Blue indicates the performance of QRF-local, orange indicates QRF-region, and green indicates QRF-national.

#### 4.4 Deterministic metrics

340 Figure 8 shows the cumulative distribution function for the deterministic metrics of Nash–Sutcliffe efficiency (NSE) and  
 Kling–Gupta efficiency (KGE) scores for mean predictions. Multi-site learning improves NSE for most catchments, but for  
 KGE, improvements are most apparent when the local approach yields low KGE values. For example, when investigating  
 catchments at the lower 25% percentile, QRF-region and QRF-national improved the median KGE by 6%. However, for  
 catchments where QRF-local provided decent KGE scores (top 25% performers), multi-site setups yielded similar scores to a  
 345 single-basin approach. This would highlight the equalizing effects of multi-site learning for QRF, as it is most impactful for  
 catchments with limited performance in the single-basin post-processing.

Figure 8 also provides deterministic metrics for the uncorrected GR6J model predictions. The figure highlights that the  
 proposed QRF methods can improve hydrological deterministic predictions, especially for NSE. For example, QRF-national  
 produced better NSE performance compared to GR6J predictions (0.87 vs 0.86 in median NSE) and for 75% of the study’s  
 350 catchments. Overall, QRF variants had better NSE for the majority of the catchments. For KGE, the uncorrected GR6J estimates  
 outperform all tested QRF approaches.

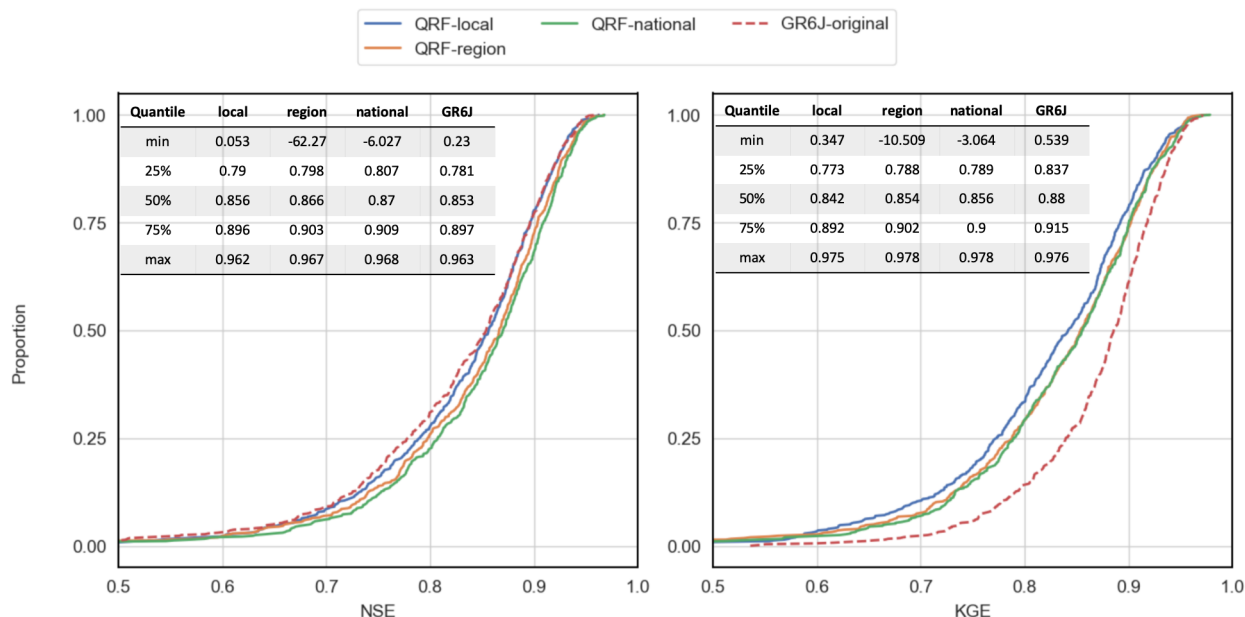


**Figure 8.** CDF of deterministic metrics across the 564 catchments for the QRF variants during the testing period. Curves that are closer to the right of the plots indicate better performance. The blue line represents the performance of mean uncertainty estimates for QRF-local, orange for QRF-region, green for QRF-national, while red represents the performance of raw GR6J predictions.

We argue that these results show: (i) the ability of QRF in its multi-site setup to identify and transfer useful information from neighbouring catchments; (ii) although the improvements relate to both deterministic and uncertainty predictions, they are most significant for coverage ratio, CRPSS, WSS, NSE, and KGE. Building on these findings, we investigated whether these benefits were more pronounced under specific hydrological conditions.

#### 4.5 How do QRF uncertainty estimates perform for different flow ranges?

Here, we aim to understand how the proposed QRF approaches perform across different flow ranges. Table 4 summarizes the average values of the alpha, dispersion, CRPSS, and interval scores for three flow groups: high ( $> 67\%Q_{med}$ ), medium ( $> 34\%Q_{med}$  and  $< 66\%Q_{med}$ ), and low flows ( $< 33\%Q_{med}$ ).

Performances were stratified based on the median values of the uncertainty distributions. Under low-flow conditions, the scores are similar, especially alpha and dispersion scores. But for higher simulated flows, multi-site QRFs provide better reliability (alpha score and coverage ratio) and better overall performance (CRPSS and WSS). Although QRF-local was able to provide narrower interval widths, especially for higher flows, it had lower reliability compared to multi-site QRFs. QRF-region and QRF-national adapt to higher-flow ranges by providing wider uncertainty estimates and enable better reliability and conditionality, as reflected in the improved CRPSS and Winkler scores.

**Table 4.** Summary of average metrics for different QRF methods across the 564 catchments of the study. Three flow ranges are included: high, medium, and low simulated flows. The bold numbers indicate better performance in each group.

Regime	QRF variant	Alpha score	Dispersion score	CRPSS	CR90.0	AWSS	WSS
Low flows ( $< 33\%Q_{med}$ )	QRF_local	<b>0.769</b>	<b>0.905</b>	0.914	0.848	<b>0.921</b>	0.919
	QRF_region	0.767	0.901	0.919	<b>0.874</b>	0.918	0.925
	QRF_national	0.765	<b>0.905</b>	<b>0.921</b>	0.871	0.920	<b>0.927</b>
Medium flows ( $> 34\%Q_{med}$ and $< 66\%Q_{med}$ )	QRF_local	0.819	<b>0.764</b>	0.792	0.862	<b>0.808</b>	0.812
	QRF_region	<b>0.833</b>	0.752	0.797	<b>0.882</b>	0.798	0.821
	QRF_national	0.831	0.758	<b>0.802</b>	<b>0.882</b>	0.802	<b>0.825</b>
High flows ( $> 67\%Q_{med}$ )	QRF_local	0.809	-0.216	0.225	0.870	<b>0.269</b>	0.381
	QRF_region	<b>0.827</b>	-0.342	0.247	0.889	0.154	0.391
	QRF_national	0.826	<b>-0.213</b>	<b>0.264</b>	<b>0.890</b>	0.249	<b>0.427</b>

#### 4.6 Impact of static descriptors

To understand the impact of static catchment descriptors, Figure 9 illustrates the distributional metrics for QRF-national and QRF-basic. QRF-basic is a multi-site QRF trained across all catchments of the study and using the same features as for QRF-local (no static features). Notable differences between the two variants are observed: in terms of reliability (median 0.827 vs. 0.806 across all catchments), sharpness (0.637 vs. 0.614), and CRPSS (0.706 vs. 0.691). Largest differences are observed for CRPSS, as QRF-national was better for 80% of the stations of the study. Furthermore, Figure F2 in Appendix F shows that QRF-basic had very similar CRPSS values as for QRF-local. These results suggest that the performance improvements in multi-site QRF models are not solely due to the inclusion of hydrological diversity in the training data. Static catchment descriptors play a significant role, and the selection of informative static features appears to be critical for effective multi-site QRF implementations.

#### 4.7 Sensitivity to scale (potential for improving the performance of QRF-national)

Following the results of the previous section, we found that multi-site learning can significantly degrade the performance for four cases across distinct hydrological regions; an example of such catchments is presented in Figure. 10. To investigate this, Table 5 presents the differences in performance (alpha score and CRPSS) between QRF-national and QRF-local based on the variability of errors  $\epsilon_t$  for three groups: group 1 is characterized by important error variability ( $>1.5$ ), group 2 also has important error variability but to a lesser degree ( $0.77 < \epsilon_t < 1.5$ ), and group 3 ( $<0.77$ ) which can be seen as having normal variability. Values 1.5 and 0.77 are the 99% and 90% quantiles of the interquartile range used to standardize the errors  $\epsilon_t$ . QRF-national performed poorly for catchments with significant variations in the target variable, with notable decreases

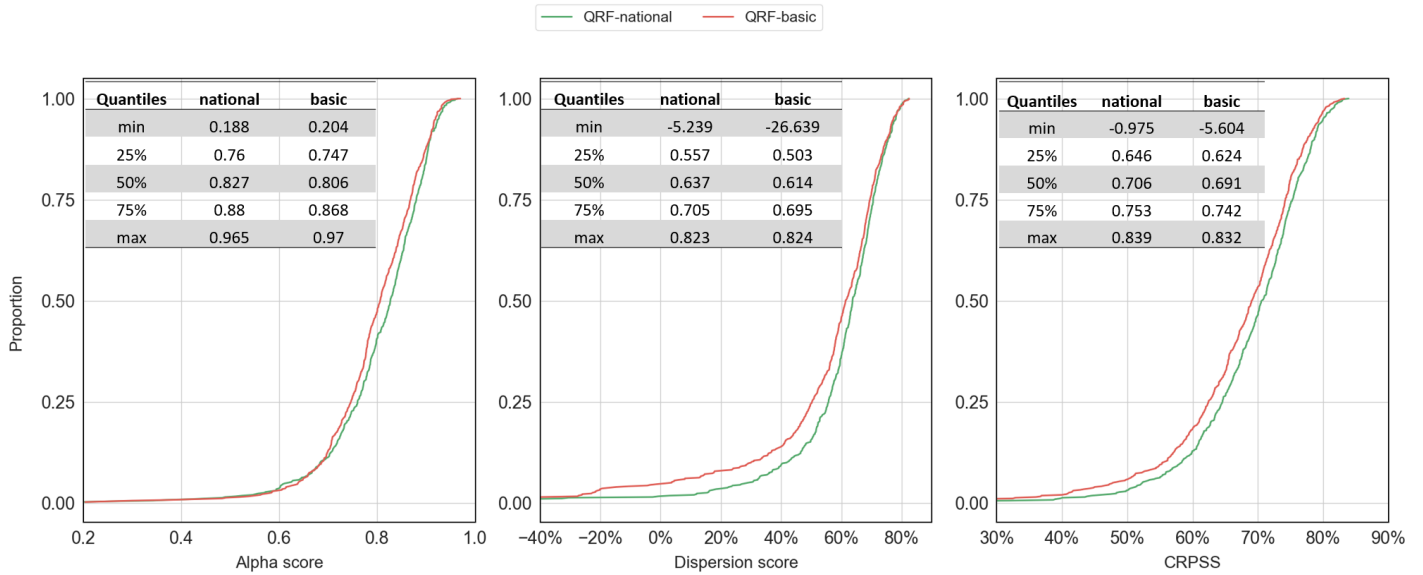


**Figure 9.** Distributional metrics across the 564 catchments for the QRF variants in the study. Curves that are closer to the right of the plots indicate better performance. The red line represents the performance of QRF-basic and green represents QRF-national.

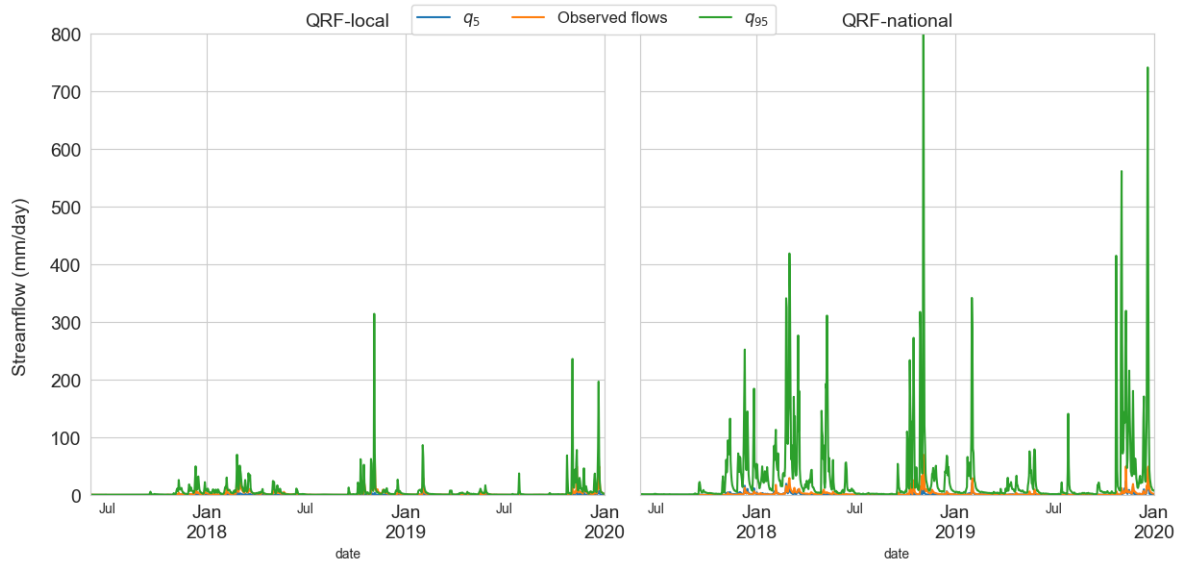


**Figure 10.** Example uncertainty estimates for a Mediterranean catchment (station Y960000102) from QRF-local (left) and QRF-national (right), covering the period from July 2017 to January 2020. The estimated 5% quantile is shown in blue, and the 95% quantile in green. The QRF-national model noticeably overestimates the upper (95%) uncertainty quantile.

in reliability and CRPSS compared to a single-basin approach. These results highlight that robust standardization of input variables and errors is key to delivering meaningful multi-site QRFs, since this enables the algorithm to find analogs from locally calibrated hydrological model inputs. Furthermore, the aforementioned scale discrepancies occurred specifically for catchments characterized by frequent zero values in simulated and observed streamflows. This can be problematic when using logarithmic relative hydrological errors. Figure. 10 illustrates QRF-local and QRF-national predictions for the 5% and 95% quantiles alongside observed flows for the Y960000102 catchment. Clearly, QRF-national overestimates the upper quantile. The local approach thus yields better results, since the error dynamics of this catchment are unconventional compared to the other catchments of the study.

**Table 5.** Average and median (shown in parentheses) differences between QRF-local and QRF-national models across distributional metrics, evaluated across different error scale groups. For catchments with extreme error variability (Group 1), QRF-national model degrades the quality of uncertainty estimates.

Error scale	Alpha score	Dispersion score	CRPSS
Group 1	-0.26 (-0.241)	-0.786 (-0.028)	-0.297 (-0.084)
Group 2	-0.023 (-0.032)	-0.091 (-0.021)	0.009 (0.011)
Group 3	0.015 (0.007)	0.01 (0.008)	0.021 (0.022)

## 5 Discussion

### 5.1 When and where is it preferable to use a multi-site learning setup?

Although training QRF on local data yields good uncertainty estimates, as discussed in previous studies (Taillardat et al., 2016; Zhang et al., 2023), using a multi-site setup can slightly improve QRF performance. Our results indicate that the best improvements are achieved with QRF-national, which includes all 564 catchments of the study. The improvements mainly concern (i) catchments where local information is not sufficient (i.e., limited QRF-local performance), (ii) CRPSS and WSS scores for nearly all catchments, and (iii) periods of higher flows.

The results presented in Section 4 indicate that multi-site learning improves the performance of QRF models, and that larger models yield better uncertainty estimates (QRF-national > QRF-region > QRF-local). We find this result interesting, since one might argue that regional models in the QRF-region approach provide an equilibrium in spatial variability by aggregating similar catchments and, possibly, similar error dynamics (Johnson et al., 2023). Such an approach confines the QRF analog search to specific hydrological regions, without extending the search to the entire study area. QRF-national, however, is not constrained by the predefined hydro-climatological regions. Region indicators are included as input features for QRF-national, and the algorithm is trained to find analogous events using these indicators, but is not strictly limited by them. Spatial variability appears to be beneficial for QRF, provided that appropriate catchment descriptors are used, and incorporating explicit measures of catchment similarity could further improve multi-site learning with QRF (Hashemi et al., 2022; Kratzert et al., 2024).

Most improvements are noted for high and medium flows. QRF-national provided a better alpha score, i.e., reliability for 60% of the catchments during high and medium flows compared to QRF-local, but performance was identical for low flows. 410 As highlighted in Bertola et al. (2023) and Auer et al. (2024), high flows are generally more difficult to predict and some high-flow events cannot be predicted exclusively from local historical data. QRF makes use of information from neighboring catchments to provide uncertainty estimates for these events that can be more challenging to predict. Local information seems to be sufficient to characterize low-flow events.

The provided analyses highlighted a limitation of the multi-site QRFs which concerns catchments characterized by frequent 415 zero flow values. Modelling hydrological model errors of ephemeral catchments is generally challenging (McInerney et al., 2019; Li et al., 2016), particularly with the use of a log-based error transformation. Figure 10 shows that multi-site learning can degrade the predictions for ephemeral catchments as uncertainties are overestimated. Although we have added the  $\delta$  offset parameter, the use of an alternative transformation that is better suited to zero flow values (e.g., a Box-Cox transformation) could better stabilize hydrological errors used to train the QRF models for ephemeral catchments. Another solution could be 420 the treatment of such catchments separately when training multi-site QRF. As showed in Figure. 10, QRF-local better managed the case of zero flow values. In the literature, other approaches (Hashemi et al., 2022; Fang et al., 2024) use adapted catchment groupings based on clustering approaches grouping homogeneous catchments. The use the number of zero flow values or the clusters as inputs to QRF can allow QRF to better distinguish catchments characterized by this issue.

Also, we expected that the proposed variants would also improve KGE as was observed in the previous studies of (Zhang 425 et al., 2023; Shen et al., 2022; Magni et al., 2023). For example, Magni et al. (2023) used a closely related deterministic RF framework for hydrological error correction and found that the hybrid RF approach boosted streamflow predictions from a median of -0.03 to 0.51. Here, the post-processing was not beneficial for KGE performances, and we suggest that this can be attributed to how QRF hyperparameters were selected. The used selection criterion in this study aims to maximize the probabilistic performances of reliability and sharpness of the uncertainty estimates. While for the aforementioned studies, the 430 RF post-processor was optimized specifically for deterministic error correction.

## 5.2 What is the importance of meaningful catchment attributes?

We showed in Figure 9 that the improvements in QRF-national depend on the use of static descriptors. A nation-wide QRF variant with no catchment attributes (identical input descriptors to the local variant) performed worse than a classic single-catchment QRF. This indicates that increasing hydrological diversity and lumping more catchment data are not the primary 435 drivers of performance improvements. The information shared within a multi-site setup is best used by the QRF algorithm in conjunction with quality catchment descriptors. This would enable better uncertainty characterization and improved analog searches in similar catchments. The catchment descriptors used are readily available in the CAMELS-FR and other CAMELS datasets, making the use of such descriptors straightforward. Furthermore, a globally parametrized QRF post-processor is able to extend its uncertainty estimates into ungauged catchments. Magni et al. (2023) found that RF is able to learn global 440 mappings and improve deterministic estimates in poorly gauged and ungauged basins. Similar improvements could be obtained

in an uncertainty estimation at ungauged catchments context, if appropriate catchment descriptors that do not rely on observed streamflows are selected.

### 5.3 Multi-site QRF for extrapolation of hydrological uncertainties

We used a large sample dataset (CAMELS-FR) to train the QRF model, and many practical hydrological applications can be interested in applying QRF post-processing to catchments not included in the training set. Our study demonstrates the ability of the QRF model to make use of hydrological information from neighbouring catchments to improve uncertainty estimates. Building on this finding, we suggest that applying a multi-site QRF, supported by appropriate catchment descriptors, to catchments outside the training set is likely to yield improved uncertainty estimates compared to a QRF model trained with single catchment data. However, the quality of these estimates remains unexplored, as the generalizability of multi-site QRF variants would depend on the similarity between hydrological model errors between the training catchments and the target regions to which uncertainty estimates are extrapolated. A spatio-temporal cross-validation experiment (Fang et al., 2024) that splits the training and testing by catchments and time periods can be used to understand the flexibility of multi-site QRF post-processing. Also, the proposed framework can be adapted for a prediction at ungauged basins. to explore this extension, the main practical difficulty lies in obtaining consistent hydrological model states for ungauged catchments, and to adapt the significant additional uncertainty usually associated with such settings (Razavi and Coulibaly, 2013; Oudin et al., 2008; Bourgin et al., 2015). If this can be properly handled, the proposed QRF multi-site variants could provide meaningful uncertainty estimates in the context of uncertainty estimation for ungauged catchments. A comparison to LSTM based post-processing techniques would be also interesting, as LSTMs perform well in ungauged basin setting [Kratzert et al. \(2018\)](#) ([Kratzert et al., 2018](#)).

### 5.4 On model complexity and computational time

Table 6 presents the number of parameters for each QRF variant, calculated as the product of the number of trees and the parameters of each tree (e.g., split thresholds, used input features). QRF-region and QRF-local exhibit a similar number of parameters, despite QRF-region providing better uncertainty estimates. In contrast, QRF-national shows a 47% increase in model complexity. This suggests that the performance gains of QRF-national come at the expense of increased computational cost which can be a drawback, especially since QRF stores not only the tree parameters but also samples used for training.

**Table 6.** Cumulative number of parameters across all models.

Model	Number of parameters
QRF-local	379M
QRF-region	364M
QRF-national	551M

RF-based algorithms are CPU-intensive and suffer from memory voracity, especially for larger datasets Taillardat and Mestre (2020). In the case of our study, we had no difficulty fitting QRF-local and QRF-region with an Intel(R) Core(TM) i7-4770 CPU

(3.40 GHz) and 16 GBs of memory. However, because of memory issues, we trained QRF-national on Jean-Zay HPC, where a single node with two CPUs (at 2.5 GHz) and 128 GBs of memory was sufficient. With this configuration, it takes on average 25 minutes to fit QRF-national with a single parameter. While training time is longer for multi-site settings, inference/prediction times are very similar to those of QRF-local.

## 6 Conclusions

In this study, we investigated the added value of multi-site learning with a hydrologically informed quantile random forest (QRF) post-processor across a large set of 564 French catchments. Three training setups were proposed – local, regional, and national – which we evaluated with different probabilistic metrics and across various hydrometeorological conditions. Based on reliability, sharpness, and overall metrics, our results indicate that multi-site learning improves QRF uncertainty estimates, with notable enhancements; (i) for overall metrics (CRPSS and WSS) and deterministic metrics (NSE and KGE) (ii) at stations where the local approach provided unreliable uncertainty estimates; and (iii) for high and medium flows, where predictions can be more challenging. These findings corroborate previous studies (Fang et al., 2024; Bertola et al., 2023; Auer et al., 2024) that found that high-flow events can have similar characteristics in neighbouring catchments. These results suggest that the QRF algorithm in its regional extensions can leverage data from neighbouring catchments to improve its uncertainty estimates; this is particularly advantageous given the off-the-shelf use of available catchment descriptors and the similarity of the learning process between local and regional variants. Additionally, the selection of representative and quality catchment attributes and static features is necessary to achieve the aforementioned improvements. We also found that using a single QRF post-processor for all catchments in the study (QRF-national) provided the best probabilistic predictions, which might indicate that the larger the model the better the uncertainty estimates with QRF. But QRF-national can yield erroneous uncertainty estimates for catchments with significant scale variations in the errors. We argue that this is mainly due to the use of logarithmic transformation of relative errors, which strongly influences hydrological error dynamics at such stations. The use of other transformations and experimenting with other catchments groupings (Hashemi et al., 2022) could solve this issue. In addition, larger models are associated with higher computational costs, with increased complexity, and with a larger number of parameters. This is particularly relevant for QRF, as RF-based algorithms are known for their intensive memory use. However, some solutions include the use of GPU-accelerated QRFs (Raschka et al., 2020).

We acknowledge certain limitations related to model-dependent artifacts. In this study, we were able to test QRF variants only using the GR6J hydrological model, as it was the only model for which simulations were available. However, the proposed framework is flexible and can be extended to other hydrological models and states. A comparison with other error models is also an attractive option, this includes standard Autoregressive models, and LSTM based error modelling. These findings highlight the performance enhancements of regional hydrologically informed QRF post-processing, and we aim to explore further in future studies the merits of the proposed QRF framework in both forecasting applications and prediction at ungauged basins.

*Author contributions.* T.E. carried out the experiments and wrote the manuscript with support from F.B.; C.P. and V.A. helped review the manuscript and supervise the project.

500 *Code and data availability.* The quantile-forest package is available at <https://pypi.org/project/quantile-forest>. The airGR package can be downloaded from CRAN repositories using the following identifier: 10.32614/CRAN.package.airGR. The evalhyd-python package can be downloaded from the HAL open archive using the following identifier: hal-04088473. The CAMELS-FR dataset can be downloaded from the Recherche Data Gouv repository using the following identifier: 10.57745/WH7FJR.

## Appendix A: Overview

505 The Appendix is structured as follows: Appendix B compares the overall performance of K-Nearest Neighbors model against QRF-local. Appendix C investigates the power transformation used to calibrate the hydrological model GR6J. Appendix D provides the distribution of the selected hyperparameters for QRF-local and QRF-region variants, Appendix E details the used assessment criteria used to compare the uncertainty quantification approaches of the study. Finally, Appendix E provides additional results that complement the main paper.

## 510 Appendix B: K-Nearest Neighbors model as benchmark

### B1 K-Nearest Neighbours algorithm

We used a naive k-nearest neighbors approach as a benchmark. The k-nearest neighbors (K-NN) algorithm is a non-parametric method that makes predictions based on the closest historical examples in the feature space. In hydrology, it is often used to estimate streamflow by averaging the outputs of the k most analogous conditions. Here analogs were used to estimate  
515 uncertainty, on a local basis. Table B1 presents the hyperparameters used for the K-NN algorithm, while table B2 compares the approaches K-NN and QRF-local. Average and median (between parentheses) across the catchments of the study, including distributional, interval and deterministic metrics.

### B2 K-Nearest Neighbours and QRF-local comparison

**Table B1.** Hyperparameters Set Optimized for K-NN approach

Hyperparameter	Values
Number of neighbors	5, 10, 25, 50, 75, 100, 150, 200, 400, 800
Distance	Uniform, distance

Table B2 compares the average and median performance metrics of QRF-local and K-NN across the 564 catchments. Overall,  
520 QRF-local consistently outperforms K-NN across all evaluated metrics. It achieves higher alpha scores, improved dispersion scores, and better CRPSS values, indicating both more reliable and more skillful probabilistic predictions. These results suggest that QRF-local leverages dynamic input features more effectively than the simpler K-NN approach.

## Appendix C: Prior transformations on streamflow

The power transformations are applied to the target variable – both observed and simulated streamflows – before calculating  
525 the associated KGE criteria (Equation C1). For example square root transformation aim at increasing the weight of errors for specific hydrological regimes. The use of streamflow transformations for model calibration is further investigated in the recent

**Table B2.** Average performance scores across the 564 catchments for QRF-local and K-NN. Median scores are shown in parentheses. Bold values indicate better performance for each metric.

Model	Alpha score	Dispersion score	CRPSS	CR90.0	AWSS	WSS	NSE	KGE
K-NN	0.771 (0.798)	0.587 (0.63)	0.655 (0.674)	0.835 (0.848)	0.678 (0.702)	0.698 (0.72)	0.825 (0.85)	0.812 (0.835)
QRF_local	<b>0.799 (0.824)</b>	<b>0.593 (0.636)</b>	<b>0.674 (0.686)</b>	<b>0.860 (0.871)</b>	<b>0.680 (0.709)</b>	<b>0.715 (0.731)</b>	<b>0.832 (0.856)</b>	<b>0.822 (0.842)</b>

study of Thirel et al. (2024)

$$\text{KGE}(Q_{\text{obs}}^p, Q_{\text{prd}}^p) = 1 - \sqrt{(r-1)^2 + (\alpha-1)^2 + (\beta-1)^2} \quad (\text{C1})$$

$$r = \frac{\text{Cov}(Q_{\text{obs}}^p, Q_{\text{prd}}^p)}{\sigma_{\text{obs}}\sigma_{\text{prd}}} \quad (\text{C2})$$

$$530 \quad \alpha = \frac{\sigma_{\text{prd}}}{\sigma_{\text{obs}}} \quad (\text{C3})$$

$$\beta = \frac{\mu_{\text{prd}}}{\mu_{\text{obs}}} \quad (\text{C4})$$

Where:  $r$  is the Pearson correlation coefficient,  $\alpha$  is the variability ratio,  $\beta$  is the bias ratio.  $\mu$  and  $\sigma$  represents the mean and standard deviation of the transformed streamflow time series.

#### Appendix D: Distribution of QRF hyperparameters for QRF-local and -region

535 Figures D1 and D2 show the distribution of hyperparameters for QRF-local and QRF-region, respectively. Unlike the national approach, which uses a single set of hyperparameters, QRF-local assigns one set per catchment, while QRF-region uses one set per region. Overall, hyperparameters vary across catchments and regions. Important variability is observed for the minimum number of samples at child nodes, which which affects trees depth. The values of this hyperparameter were mostly skewed toward lower ranges for both QRF-local and QRF-region. The response of QRF-local to the other hyperparameters was less  
540 discriminative. For QRF-local, the selected values for the number of trees and features per split remained largely consistent across the values tested. For QRF-region, 200 trees were most often selected, while 8 features and the default square root (6 features per split) were the most frequent optimal value for the number of features per split hyperparameter.

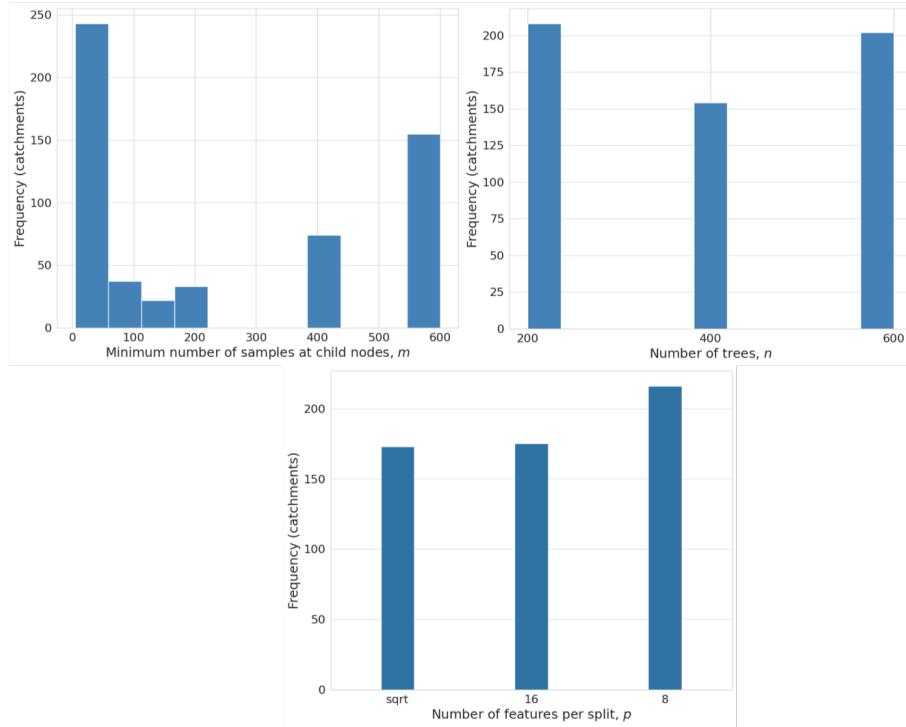


**Figure D1.** Distribution of the selected hyperparameters for QRF-local across the catchments of the study. The hyperparameters are: (i) The number of trees  $n$ , (ii) The minimum number of samples at child nodes  $m$ , and (iii) The number of features per split,  $p$

## Appendix E: Assessment criteria

### E1 Continuous ranked probability score

545 Given a univariate predictive distribution  $F$  and a corresponding realization  $y$ , the continuous ranked probability score (CRPS) is defined as:

$$\text{CRPS}(F, y) = \int_{-\infty}^{+\infty} (F(u) - H(u - y))^2 du, \quad (\text{E1})$$

where  $H$  is the Heaviside function such that  $H(u - y) = 1$  if  $u \geq y$  and 0 otherwise. In this study, the probabilistic predictions are in the form of draws distributions; hence, equation E1 has to be discretized for computation. We apply the method which is implemented in the function “CRPS\_FROM\_ECDF” from the Python package EvalHyd (Hallouin et al., 2023). The CRPS is negatively oriented, meaning that smaller values are better.

550

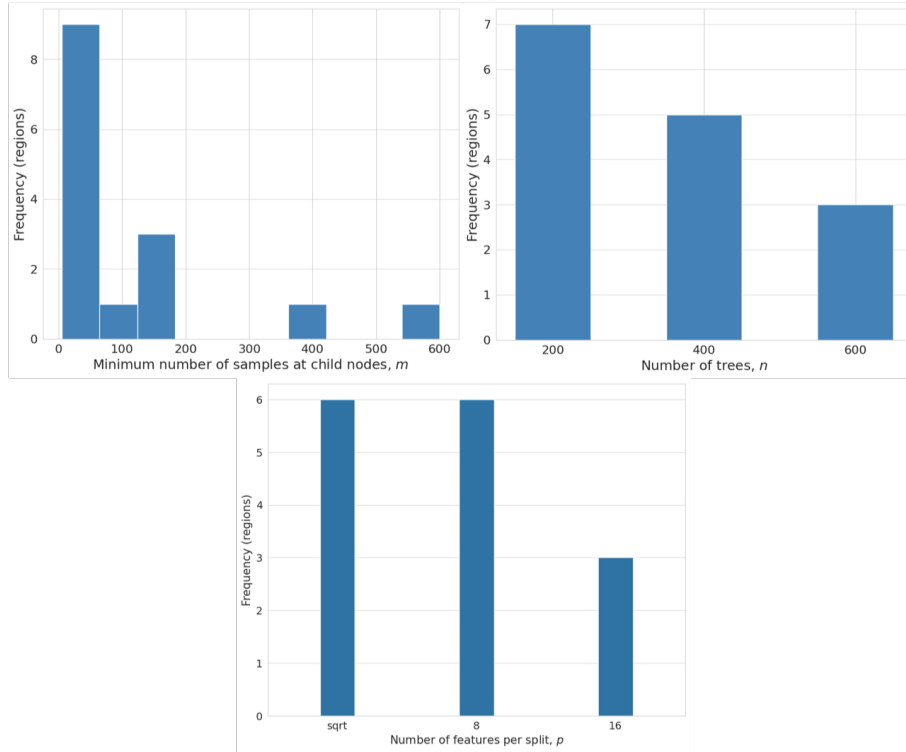


**Figure D2.** Distribution of the selected hyperparameters for QRF-region across the hydroclimatological catchment groups used in the study. The hyperparameters are: (i) The number of trees  $n$ , (ii) The minimum number of samples at child nodes  $m$ , and (iii) The number of features per split,  $p$

## E2 Skill score

The performance of predictions can be more easily compared with that of a reference prediction skill scores. Skill scores (SS) are used to assess the relative quality of two predictions. They are generally defined as:  $SS$  it is generally defined as:

$$555 \quad SS = 1 - \frac{\bar{S}}{\bar{S}_{\text{ref}}} \quad (\text{E2})$$

where  $\bar{S}$  and  $\bar{S}_{\text{ref}}$  are the scores of predictions from the model to evaluate and the reference model respectively. Climatology is commonly used as a reference. In this study, we consider climatological distributions of observed streamflows. It has been estimated as the empirical distribution of discharges across the training periods (P1).

## E3 Alpha score

560 Given a univariate forecast distribution  $F_t$  and a corresponding realization  $y_t$ , the p value is  $F_t(x_t) = p(Y_t \leq y_t)$  and the alpha score is defined as:

$$\alpha'_y = \frac{1}{N_y} \sum_{i=1}^{N_y} |p_{y(i)} - p_{y(i)}^{(th)}| \quad (\text{E3})$$

where  $p_y^{(i)}$  and  $p_y(i)^{(th)}$  are the  $i$ th observed and theoretical p values of  $y_t$  values.  $N_y$  is the number of  $y_t$  values. The alpha score takes values between 0 and 1. It is positively oriented, with scores close to 1 reflecting perfect reliability.

565 The performance of streamflow forecasts can vary depending on the flow range considered (e.g., flood forecasting vs. drought forecasting). Bellier et al. (2017) suggest a forecast-based sample stratification for continuous scalar variables in order to consider the merits of streamflow forecasts on different ranges of flows. To ensure robust reliability estimates and prevent potential compensation effects, the alpha score was calculated separately for three distinct flow ranges: low, high, and average forecasted flows.

#### 570 **E4 Dispersion score**

Sharpness is quantified with the skill score of the forecast CRPS of median forecasts relative to climatological streamflow distribution, in which CRPS median is defined as follows:

$$CRPS_{median}(F) = CRPS(F, F_{median}) \quad (\text{E4})$$

575 where  $F_{median}$  is the median value of the distribution  $F$ . This is related to an interesting decomposition of the CRPS proposed in the PhD thesis of Bontron (2004)

#### **E5 Coverage ratio**

Given a predictive interval  $[L_t, U_t]$  at a confidence level  $1 - \alpha$  and a corresponding observation  $y_t$ , the coverage ratio (CR) is defined as:

$$CR = \frac{1}{N} \sum_{t=1}^N \mathbf{1}\{y_t \in [L_t, U_t]\}, \quad (\text{E5})$$

580 where  $\mathbf{1}\{\cdot\}$  is the indicator function and  $N$  is the number of observations.

#### **E6 Average width**

The average width (AW) of the prediction intervals is given by:

$$AW = \frac{1}{N} \sum_{t=1}^N (U_t - L_t), \quad (\text{E6})$$

quantifying the sharpness of the probabilistic forecasts.

The Winkler score (WS) penalizes both miscoverage and interval width and is defined as:

$$WS_t = (U_t - L_t) + \frac{2}{\alpha}(L_t - y_t)\mathbf{1}\{y_t < L_t\} + \frac{2}{\alpha}(y_t - U_t)\mathbf{1}\{y_t > U_t\}, \quad (\text{E7})$$

and the overall score is averaged over all observations:  $WS = \frac{1}{N} \sum_{t=1}^N WS_t$ .

## Appendix F: Results supplement

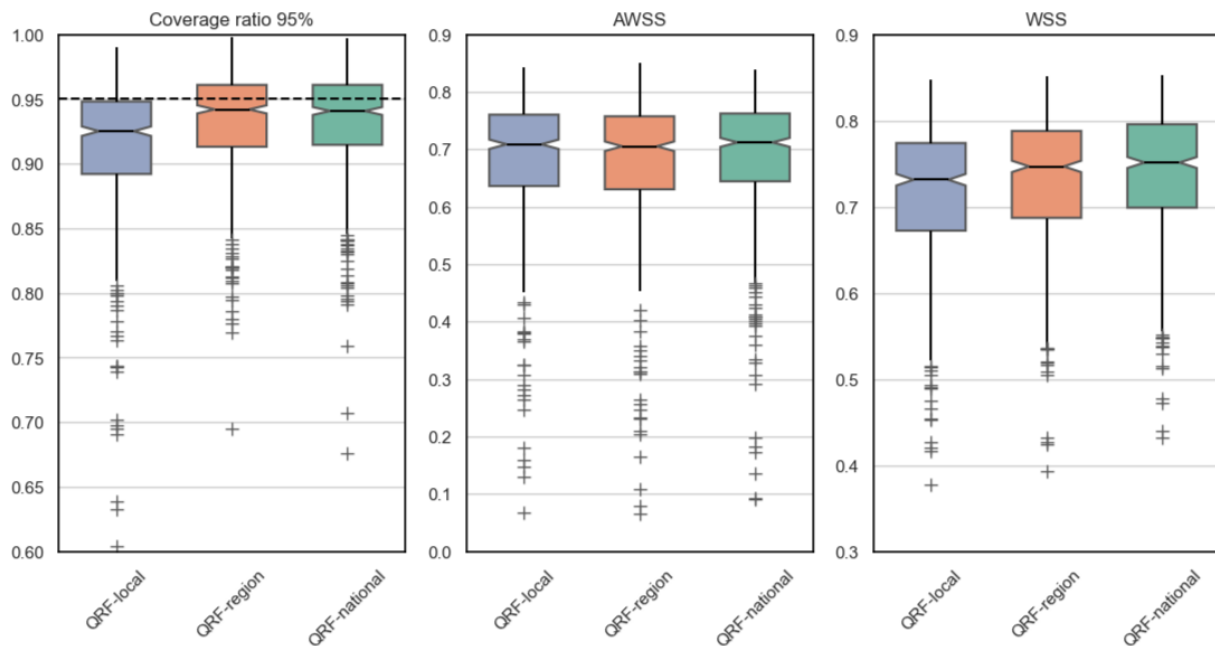


**Figure F1.** Box plots of 95% interval-based metrics across the 564 catchments of the study. Blue for the performance of QRF-local, orange for QRF-region, and green for QRF-national.

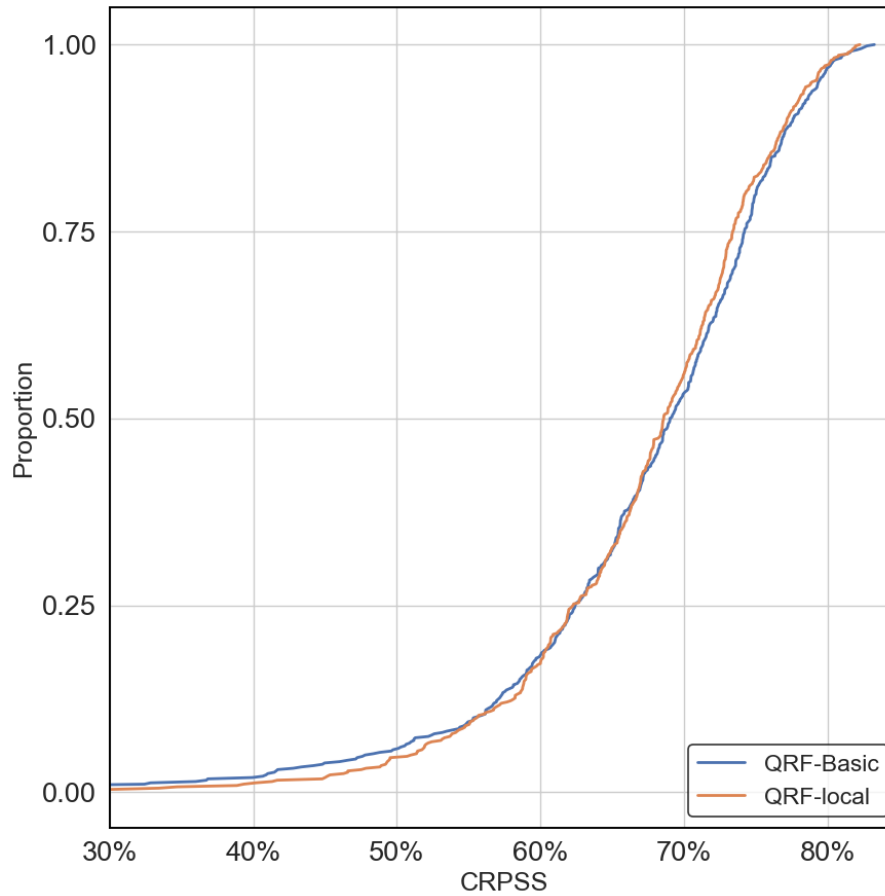


**Figure F2.** CRPSS metric across the 564 catchments. The blue line represents the performance of QRF-basic, orange represents QRF-local.

590 *Competing interests.* The authors declare that they have no conflict of interest.

*Acknowledgements.* We gratefully acknowledge Météo-France for providing the weather data and SCHAPI for the streamflow data. We would also like to thank the PREMHYCE and CIPRHES projects (ANR-20-CE04-0009), OFB, INRAE and SCHAPI for their financial support to the first author, which made this research possible. This work was performed using HPC resources from GENCI-IDRIS (Grant 2024-AD011013991R2).

595 **References**

- Auer, A., Gauch, M., Kratzert, F., Nearing, G., Hochreiter, S., and Klotz, D.: A data-centric perspective on the information needed for hydrological uncertainty predictions, *Hydrology and Earth System Sciences*, 28, 4099–4126, <https://doi.org/10.5194/hess-28-4099-2024>, 2024.
- Bates, B. C. and Campbell, E. P.: A Markov chain Monte Carlo scheme for parameter estimation and inference in conceptual rainfall-runoff modeling, *Water resources research*, 37, 937–947, 2001.
- Bellier, J., Zin, I., and Bontron, G.: Sample stratification in verification of ensemble forecasts of continuous scalar variables: Potential benefits and pitfalls, *Monthly Weather Review*, 145, 3529–3544, <https://doi.org/10.1175/MWR-D-16-0487.1>, 2017.
- Bennett, J. C., Robertson, D. E., Wang, Q. J., Li, M., and Perraud, J.-M.: Propagating reliable estimates of hydrological forecast uncertainty to many lead times, *Journal of Hydrology*, 603, 126 798, <https://doi.org/10.1016/j.jhydrol.2021.126798>, 2021.
- 605 Bertola, M., Blöschl, G., Bohac, M., Borga, M., Castellarin, A., Chirico, G., Claps, P., Dallan, E., Danilovich, I., Ganora, D., et al.: Megafloods in Europe can be anticipated from observations in hydrologically similar catchments, *Nat. Geosci.*, 16, 982–988, 2023.
- Bontron, G.: Prévision quantitative des précipitations: Adaptation probabiliste par recherche d’analogues. Utilisation des Réanalyses NCEP/NCAR et application aux précipitations du Sud-Est de la France, Ph.D. thesis, Institut National Polytechnique Grenoble (INPG), 2004.
- 610 Bourgin, F., Andréassian, V., Perrin, C., and Oudin, L.: Transferring global uncertainty estimates from gauged to ungauged catchments, *Hydrology and Earth System Sciences*, 19, 2535–2546, 2015.
- Breiman, L.: Random forests, *Machine learning*, 45, 5–32, 2001.
- Breiman, L., Friedman, J., Olshen, R. A., and Stone, C. J.: *Classification and regression trees*, Routledge, 2017.
- Coron, L., Thirel, G., Delaigue, O., Perrin, C., and Andréassian, V.: The Suite of Lumped GR Hydrological Models in an R package, *Environmental Modelling and Software*, 94, 166–171, <https://doi.org/10.1016/j.envsoft.2017.05.002>, 2017.
- 615 Coron, L., Delaigue, O., Thirel, G., Dorchie, D., Perrin, C., and Michel, C.: airGR: Suite of GR Hydrological Models for Precipitation-Runoff Modelling, <https://doi.org/10.15454/EX11NA>, r package version 1.7.4, 2023.
- Delaigue, O., Guimarães, G., Brigode, P., Génot, B., Perrin, C., Soubeyroux, J., Janet, B., Addor, N., and Andréassian, V.: CAMELS-FR dataset: A large-sample hydroclimatic dataset for France to explore hydrological diversity and support model benchmarking, submitted to
- 620 ESSD, <https://doi.org/10.57745/WH7FJR>, 2024.
- Delle Monache, L., Eckel, F. A., Rife, D. L., Nagarajan, B., and Searight, K.: Probabilistic weather prediction with an analog ensemble, *Monthly Weather Review*, 141, 3498–3516, 2013.
- Dufeu, E., Mougin, F., Foray, A., Baillon, M., Lamblin, R., Hebrard, F., Chaleon, C., Romon, S., Cobos, L., Gouin, P., et al.: Finalisation de l’opération HYDRO 3 de modernisation du système d’information national des données hydrométriques, *LHB*, 108, 2099 317, <https://doi.org/10.1080/27678490.2022.2099317>, 2022.
- 625 Evin, G., Thyer, M., Kavetski, D., McInerney, D., and Kuczera, G.: Comparison of joint versus postprocessor approaches for hydrological uncertainty estimation accounting for error autocorrelation and heteroscedasticity, *Water Resources Research*, 50, 2350–2375, 2014.
- Fang, S., Johnson, J. M., Yeghiazarian, L., and Sankarasubramanian, A.: Improved national-scale above-normal flow prediction for gauged and ungauged basins using a spatio-temporal hierarchical model, *Water Resources Research*, 60, e2023WR034 557, 2024.
- 630 Georgakakos, K. P., Seo, D.-J., Gupta, H., Schaake, J., and Butts, M. B.: Towards the characterization of streamflow simulation uncertainty through multimodel ensembles, *Journal of hydrology*, 298, 222–241, 2004.

- Gneiting, T., Raftery, A. E., Westveld, A. H., and Goldman, T.: Calibrated Probabilistic Forecasting Using Ensemble Model Output Statistics and Minimum CRPS Estimation, *Monthly Weather Review*, 133, 1098–1118, <https://doi.org/10.1175/MWR2904.1>, 2005.
- Gneiting, T., Balabdaoui, F., and Raftery, A. E.: Probabilistic forecasts, calibration and sharpness, *Journal of the Royal Statistical Society Series B: Statistical Methodology*, 69, 243–268, 2007.
- 635 Golian, S., Murphy, C., and Meresa, H.: Regionalization of hydrological models for flow estimation in ungauged catchments in Ireland, *Journal of Hydrology: Regional Studies*, 36, 100 859, 2021.
- Gupta, A., Hantush, M. M., Govindaraju, R. S., and Beven, K.: Evaluation of hydrological models at gauged and ungauged basins using machine learning-based limits-of-acceptability and hydrological signatures, *Journal of Hydrology*, 641, 131 774, 2024.
- 640 Gupta, H. V., Kling, H., Yilmaz, K. K., and Martinez, G. F.: Decomposition of the mean squared error and NSE performance criteria: Implications for improving hydrological modelling, *Journal of Hydrology*, 377, 80–91, 2009.
- Hallouin, T., Bourgin, F., Perrin, C., Ramos, M.-H., and Andréassian, V.: evalhyd v0. 1.1: a polyglot tool for the evaluation of deterministic and probabilistic streamflow predictions, *EGUsphere*, 2023, 1–23, 2023.
- Hashemi, R., Brigode, P., Garambois, P.-A., and Javelle, P.: How can we benefit from regime information to make more effective use of long short-term memory (LSTM) runoff models?, *Hydrology and Earth System Sciences*, 26, 5793–5816, 2022.
- 645 Hastie, T., Tibshirani, R., and Friedman, J.: *The Elements of Statistical Learning*, Springer Series in Statistics, Springer New York Inc., New York, NY, USA, 2001.
- Hu, W., Cervone, G., Young, G., and Delle Monache, L.: Machine learning weather analogs for near-surface variables, *Boundary-Layer Meteorology*, 186, 711–735, 2023.
- 650 Hwang, J., Orenstein, P., Cohen, J., Pfeiffer, K., and Mackey, L.: Improving subseasonal forecasting in the western US with machine learning, in: *Proceedings of the 25th ACM SIGKDD International Conference on Knowledge Discovery & Data Mining*, pp. 2325–2335, 2019.
- Jehn, F. U., Bestian, K., Breuer, L., Kraft, P., and Houska, T.: Using hydrological and climatic catchment clusters to explore drivers of catchment behavior, *Hydrology and Earth System Sciences*, 24, 1081–1100, 2020.
- Johnson, J. M., Fang, S., Sankarasubramanian, A., Rad, A. M., Kindl da Cunha, L., Jennings, K. S., Clarke, K. C., Mazrooei, A., and 655 Yeghiazarian, L.: Comprehensive analysis of the NOAA National Water Model: A call for heterogeneous formulations and diagnostic model selection, *Journal of Geophysical Research: Atmospheres*, 128, e2023JD038 534, 2023.
- Johnson, R. A.: quantile-forest: A Python Package for Quantile Regression Forests, *Journal of Open Source Software*, 9, 5976, <https://doi.org/10.21105/joss.05976>, 2024.
- Kling, H., Fuchs, M., and Paulin, M.: Runoff conditions in the upper Danube basin under an ensemble of climate change scenarios, *Journal of Hydrology*, 424, 264–277, 2012.
- 660 Kratzert, F., Klotz, D., Brenner, C., Schulz, K., and Herrnegger, M.: Rainfall–runoff modelling using long short-term memory (LSTM) networks, *Hydrology and Earth System Sciences*, 22, 6005–6022, 2018.
- Kratzert, F., Gauch, M., Klotz, D., and Nearing, G.: HESS Opinions: Never train a Long Short-Term Memory (LSTM) network on a single basin, *Hydrology and Earth System Sciences*, 28, 4187–4201, 2024.
- 665 Krzysztofowicz, R.: Bayesian theory of probabilistic forecasting via deterministic hydrologic model, *Water Resources Research*, 35, 2739–2750, 1999.
- Kuczera, G. and Parent, E.: Monte Carlo assessment of parameter uncertainty in conceptual catchment models: the Metropolis algorithm, *Journal of hydrology*, 211, 69–85, 1998.

- 670 Leleu, I., Tonnelier, I., Puechberty, R., Gouin, P., Viquendi, I., Cobos, L., Foray, A., Baillon, M., and Ndimba, P.-O.: La refonte du système d'information national pour la gestion et la mise à disposition des données hydrométriques, *La Houille Blanche*, 100, 25–32, <https://doi.org/10.1051/lhb/2014004>, 2014.
- Li, M., Wang, Q., Bennett, J. C., and Robertson, D. E.: Error reduction and representation in stages (ERRIS) in hydrological modelling for ensemble streamflow forecasting, *Hydrology and Earth System Sciences*, 20, 3561–3579, 2016.
- Louppe, G.: *Understanding random forests: From theory to practice*, Université de Liège (Belgium), 2014.
- 675 Magni, M., Sutanudjaja, E. H., Shen, Y., and Karssenber, D.: Global streamflow modelling using process-informed machine learning, *Journal of Hydroinformatics*, 25, 1648–1666, 2023.
- McInerney, D., Kavetski, D., Thyer, M., Lerat, J., and Kuczera, G.: Benefits of explicit treatment of zero flows in probabilistic hydrological modeling of ephemeral catchments, *Water Resources Research*, 55, 11 035–11 060, 2019.
- Meinshausen, N. and Ridgeway, G.: Quantile regression forests., *Journal of machine learning research*, 7, 2006.
- 680 Montero-Manso, P. and Hyndman, R. J.: Principles and algorithms for forecasting groups of time series: Locality and globality, *International Journal of Forecasting*, 37, 1632–1653, 2021.
- Nash, J. E. and Sutcliffe, J. V.: River flow forecasting through conceptual models part I—A discussion of principles, *Journal of Hydrology*, 10, 282–290, 1970.
- Oshiro, T. M., Perez, P. S., and Baranauskas, J. A.: How many trees in a random forest?, in: *International workshop on machine learning and data mining in pattern recognition*, pp. 154–168, Springer, 2012.
- Oudin, L., Hervieu, F., Michel, C., Perrin, C., Andréassian, V., Anctil, F., and Loumagne, C.: Which potential evapotranspiration input for a lumped rainfall–runoff model?: Part 2—Towards a simple and efficient potential evapotranspiration model for rainfall–runoff modelling, *Journal of Hydrology*, 303, 290–306, 2005.
- Oudin, L., Andréassian, V., Perrin, C., Michel, C., and Le Moine, N.: Spatial proximity, physical similarity, regression and ungauged catchments: A comparison of regionalization approaches based on 913 French catchments, *Water resources research*, 44, 2008.
- 690 Papacharalampous, G. and Langousis, A.: Probabilistic water demand forecasting using quantile regression algorithms, *Water Resources Research*, 58, e2021WR030 216, 2022.
- Pham, L. T., Luo, L., and Finley, A. O.: Evaluation of Random Forest for short-term daily streamflow forecast in rainfall and snowmelt driven watersheds, *Hydrology and Earth System Sciences Discussions*, 2020, 1–33, 2020.
- 695 Poncelet, C., Merz, R., Merz, B., Parajka, J., Oudin, L., Andréassian, V., and Perrin, C.: Process-based interpretation of conceptual hydrological model performance using a multinational catchment set, *Water Resources Research*, 53, 7247–7268, 2017.
- Pushpalatha, R., Perrin, C., Le Moine, N., Mathevet, T., and Andréassian, V.: A downward structural sensitivity analysis of hydrological models to improve low-flow simulation, *Journal of Hydrology*, 411, 66–76, <https://doi.org/10.1016/j.jhydrol.2011.09.034>, 2011.
- Pushpalatha, R., Perrin, C., Moine, N. L., and Andréassian, V.: A review of efficiency criteria suitable for evaluating low-flow simulations, *Journal of Hydrology*, 420–421, 171–182, <https://doi.org/https://doi.org/10.1016/j.jhydrol.2011.11.055>, 2012.
- 700 Raschka, S., Patterson, J., and Nolet, C.: *Machine Learning in Python: Main developments and technology trends in data science, machine learning, and artificial intelligence*, arXiv preprint arXiv:2002.04803, 2020.
- Razavi, T. and Coulibaly, P.: Streamflow prediction in ungauged basins: review of regionalization methods, *Journal of hydrologic engineering*, 18, 958–975, 2013.
- 705 Renard, B., Kavetski, D., Kuczera, G., Thyer, M., and Franks, S. W.: Understanding predictive uncertainty in hydrologic modeling: The challenge of identifying input and structural errors, *Water Resources Research*, 46, <https://doi.org/10.1029/2009WR008328>, 2010.

- Shen, Y., Ruijsch, J., Lu, M., Sutanudjaja, E. H., and Karssenber, D.: Random forests-based error-correction of streamflow from a large-scale hydrological model: Using model state variables to estimate error terms, *Computers & Geosciences*, 159, 105 019, 2022.
- Solomatine, D. P. and Shrestha, D. L.: A novel method to estimate model uncertainty using machine learning techniques, *Water Resources Research*, 45, <https://doi.org/https://doi.org/10.1029/2008WR006839>, 2009.
- 710 Taillardat, M. and Mestre, O.: From research to applications—examples of operational ensemble post-processing in France using machine learning, *Nonlinear Processes in Geophysics*, 27, 329–347, 2020.
- Taillardat, M., Mestre, O., Zamo, M., and Naveau, P.: Calibrated ensemble forecasts using quantile regression forests and ensemble model output statistics, *Monthly Weather Review*, 144, 2375–2393, 2016.
- 715 Tanguy, M., Chevuturi, A., Marchant, B. P., Mackay, J. D., Parry, S., and Hannaford, J.: How will climate change affect the spatial coherence of streamflow and groundwater droughts in Great Britain?, *Environmental Research Letters*, 18, 064 048, 2023.
- Teja, K. N., Manikanta, V., Das, J., and Umamahesh, N.: Enhancing the predictability of flood forecasts by combining Numerical Weather Prediction ensembles with multiple hydrological models, *Journal of Hydrology*, 625, 130 176, 2023.
- Thirel, G., Santos, L., Delaigue, O., and Perrin, C.: On the use of streamflow transformations for hydrological model calibration, *Hydrology and Earth System Sciences*, 28, 4837–4860, 2024.
- 720 Tiberi-Wadier, A.-L., Goutal, N., Ricci, S., Sergent, P., Taillardat, M., Bouttier, F., and Monteil, C.: Strategies for hydrologic ensemble generation and calibration: On the merits of using model-based predictors, *Journal of Hydrology*, 599, 126 233, 2021.
- Todini, E.: A model conditional processor to assess predictive uncertainty in flood forecasting, *International Journal of River Basin Management*, 6, 123–137, <https://doi.org/10.1080/15715124.2008.9635342>, 2008.
- 725 Troin, M., Arsenault, R., Wood, A. W., Brissette, F., and Martel, J.-L.: Generating ensemble streamflow forecasts: A review of methods and approaches over the past 40 years, 2021.
- Tyralis, H. and Papacharalampous, G.: A review of predictive uncertainty estimation with machine learning, *Artificial Intelligence Review*, 57, 94, 2024.
- Tyralis, H., Papacharalampous, G., Burnetas, A., and Langousis, A.: Hydrological post-processing using stacked generalization of quantile regression algorithms: Large-scale application over CONUS, *Journal of Hydrology*, 577, 123 957, 2019.
- 730 Valéry, A., Andréassian, V., and Perrin, C.: ‘As simple as possible but not simpler’: What is useful in a temperature-based snow-accounting routine? Part 2—Sensitivity analysis of the Cemaneige snow accounting routine on 380 catchments, *Journal of hydrology*, 517, 1176–1187, <https://doi.org/10.1016/j.jhydrol.2014.04.058>, 2014.
- Vidal, J.-P., Martin, E., Franchisteguy, L., Baillon, M., and Soubeyroux, J.-M.: A 50-year high-resolution atmospheric reanalysis over France with the Safran system, *International Journal of Climatology*, 30, <https://doi.org/10.1002/joc.2003>, 2010.
- 735 Wani, O., Beckers, J. V., Weerts, A. H., and Solomatine, D. P.: Residual uncertainty estimation using instance-based learning with applications to hydrologic forecasting, *Hydrology and Earth System Sciences*, 21, 4021–4036, 2017.
- White, C. J., Carlsen, H., Robertson, A. W., Klein, R. J., Lazo, J. K., Kumar, A., Vitart, F., Coughlan de Perez, E., Ray, A. J., Murray, V., et al.: Potential applications of subseasonal-to-seasonal (S2S) predictions, *Meteorological applications*, 24, 315–325, 2017.
- 740 Zhang, Y., Ye, A., Analui, B., Nguyen, P., Sorooshian, S., Hsu, K., and Wang, Y.: Comparing quantile regression forest and mixture density long short-term memory models for probabilistic post-processing of satellite precipitation-driven streamflow simulations, *Hydrology and Earth System Sciences*, 27, 4529–4550, 2023.